THESIS

CHARACTERIZATION OF A PLASMA REACTOR DEVICE FOR PHOTOVOLTAIC APPLICATIONS

Submitted by

Garrett Eugene Metz

Department of Mechanical Engineering

In partial fulfillment of the requirements

For the Degree of Master of Science

Colorado State University

Fort Collins, Colorado

Fall 2012

Master's Committee:

Advisor: John D. Williams

Leonard Mahoney
Walajabad S. Sampath
Steve Robinson

ABSTRACT

CHARACTERIZATION OF A PLASMA REACTOR DEVICE FOR PHOTOVOLTAIC APPLICATIONS

Heated pocket deposition (HPD) sources are used for the rapid manufacture of thin film CdS/CdTe photovoltaic devices. Standard lab devices produced at CSU by the HPD process have achieved efficiencies of 13%. New process methods are required to further improve the quality of the films, increase cell efficiency, and reduce production costs. A plasma-enhanced, close-spacing sublimation (PECSS) technique has recently been developed as a candidate process method. It has been successfully used to eliminate pin holes, to dope CdS with oxygen, and dope CdTe absorption layers; all of which have resulted in higher device efficiencies. In this work we present measurements describing the properties of the PECSS plasma. Specifically the uniformity of the ion current flux to the substrate is presented for nitrogen/oxygen and argon feed gases by means of in situ surface probes fabricated by segmenting a transparent conductive oxide film that is laid over the glass. Plasma properties within the PECSS processing chamber are also presented including plasma density, electron temperature, and plasma potential. Operational characteristics and scaling of PECSS are presented for pressures of 100-300 mTorr and surface areas of 160 – 1700 cm^2. A three-dimensional model was developed to calculate plasma production and transport processes, and to gain a greater understanding of the role of energetic primaries versus bulk cold electrons on spatial ionization rates that develop within the PECSS plasma as a function of gas pressure and geometry. Comparisons between the model and experimental measurements are presented and good agreement has been observed when the appropriate spatially varying ionization rates are estimated. This work

also presents the development of a diagnostic test bed that will be useful for future work in the development and understanding of the PECSS technique.

ACKNOWLEDGEMENTS

Firstly I would like to thank my advisor Dr. John Williams for allowing me the opportunity to work in his lab, his infectious taste for knowledge and support in this research has been unbelievable. Thanks to my committee for giving their time and knowledge in the support of the research in this thesis. I would like to specifically thank Dr. Leonard Mahoney for his support in the numerical modeling presented in this thesis; I truly appreciate you sharing your knowledge. Sara, without your love and support throughout my work I would not be where I am today. I would also like to thank my family and friends for their support throughout my educational journey. To my colleagues in both the CEPPE and Photovoltaic Labs, the discussions of new ideas and support in this research have been invaluable. This research was supported by the NSF-AIR program.

TABLE OF CONTENTS

CHAPTER 1: INTRODUCTION

Plasmas are a collection of electrons, ions, and neutrals in the gaseous state, and they are used in a variety of applications including thin film processing. Plasmas can be formed in many ways including electrodes powered by RF (capacitive and inductive) [Hopwood (1992), Anders (2005)], microwave [Croslyn et al (1997)], and DC-DC Pulsed [Conrad et al (2000)] power supplies. In DC glow discharge plasmas a wire or plate is biased to a voltage positive of a cathode electrode. The plasma formed in DC glow discharges are used in items such as neon signs, fluorescent lights, and plasma televisions. This thesis is concerned with characterizing plasma formed within heated pocket deposition geometries used in the production of thin film photovoltaic (PV) cells. Background information on DC glow discharges that are enhanced by hollow cathode electrostatic confinement of electrons is presented below, followed by a discussion on the focus of this thesis.

1.1 Background

Many studies have been performed on wire anode discharges [McClure G.W. (1963)], also commonly referred to as saddle field discharges [McIlraith et al (1966)] and wire ion plasma sources [Harvey et al (1987)]. The typical, most studied, configuration of the wire anode discharge is that of a cylindrical tube held at cathode potential with a thin wire held at anode potential that is passed down the centerline of the tube. In addition to plasma production, these discharges have been used for DC and pulsed-DC electron and ion beam formation [Chalise et al (2003)]. More recently Gueroult et al (2010) describe a model of a wire-induced plasma source operated in a low pressure mode. They demonstrate that when the electron mean free path exceeds the physical length of the discharge chamber effective confinement of

the primary electrons occurs and enhances plasma production rates. Their model also confirmed the general operational characteristics of previous experimental and theoretical work on these discharges with one important finding being that ions strike the cathode wall with an energy corresponding to the anode-to-cathode potential difference. These ions produce secondary electrons, which are in turn accelerated from cathode potential into the positively biased plasma region where they ionize neutrals, heat plasma electrons, and sustain the plasma. These energetic electrons are also referred to as primary electrons. In subsequent work, Gueroult et al (2011) employed a retarding potential analyzer to confirm experimentally that energetic ions were striking the cathode surfaces. These ions can sputter and subsequently texture the cathode. Neutrals excited to metastable states by primary and plasma electrons can come in contact with the cathode and drive surface modifications. Diatomic and polyatomic neutrals can be dissociated into atoms and radicals through action by primary and plasma electrons and also drive surface changes. Finally photons produced by emission from excited neutrals in the bulk plasma can cause surface effects. Constituents within cold plasmas are not in thermodynamic equilibrium and electron temperatures are significantly higher than gas, ion, radical, and ion temperatures. The many constituents that appear in glow discharges are shown in Figure 1-1 [Tanarro et al (2007)]. The strong electrostatic trapping of electrons in hollow cathode and saddle field plasma reactors, leads to increased plasma densities and enhanced ionization, dissociation, excitation, and sputter rates. Similar transparent anode DC plasma discharges can be created with plate anodes located outside of the cathode cavity. This type of configuration is often referred to as a hollow

cathode, and are advantageous because they do not require complex source design nor the use of magnets.

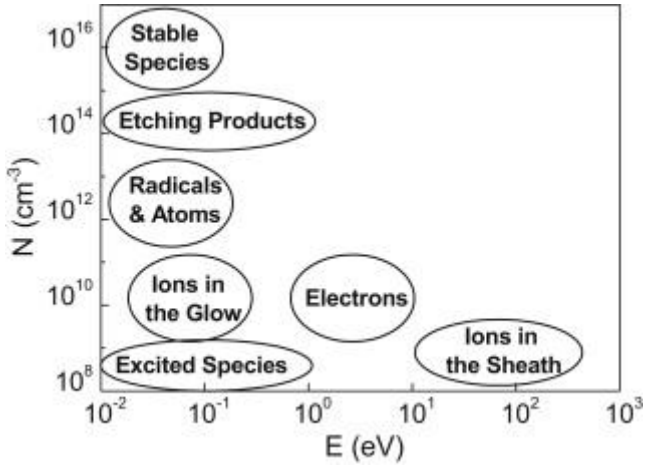

Figure 1-1. Typical species concentrations found in glow discharges as described by Tanarro et al (2011)

Hollow cathode-formed plasma has also been used to enhance the formation of films made by chemical vapor deposition (CVD). Increased photovoltaic (PV) efficiencies were gained through plasma enhanced CVD (PECVD), as described by A. Shah et al (1999) in crystalline silicon solar cells. Efficiencies in their cells went up from 8.5% to 10.1% with plasma treatment. Rech et al (2003) used large area PECVD to create thin film microcrystalline silicon solar cells and showed scaling up to substrate sizes of 30 cm x 30 cm. In a similar study, Johnson et al (2008) examined the effects of substrate bias on the growth of microcrystalline silicon to determine the useful operating regime of very large area reactors with substrates up to 500 cm^2, pressures ranging from 100 to 300 mTorr, and electrical biases from 100 to 250 V. Saddle field discharges have also been used to assist the deposition of hydrogenated amorphous carbon films, as explained by Sagnes et al (1999). In their study the cathode consisted of two

parallel plates acting as substrate holders which were placed on either side of a wire anode. Hollow cathode inspired geometries have also been used to texturize metal surfaces for biomedical applications [Riedel et al (2012), Riedel (2012)], large area surface treatments and depositions on polyethylene, tapes and wires [Barankova et al (2001), Koch et al (1991)], and in non-PV related chemical vapor deposition processes [Singh et al (1988), Bardos et al (1997), Joo (2011)]. Hollow cathode discharges have also been used by Schrittwieser et al (2010) as a means for low cost titanium sputtering.

The voltage bias applied to the anode to initiate plasma production, known as the breakdown voltage, can be very large depending on electrode configuration. The Paschen curve describes the breakdown voltages for different process gases based on pressure and electrode separation distance (Pd). Urai et al (1997) described a pulsed hollow cathode discharge in which the breakdown voltage of the source was lower than the value expected from the Paschen curve for several process gases. This is important because lower breakdown voltages will cause less stress on operating equipment.

In our group, Swanson et al (2012a) recently used a plasma-enhanced close-spacing sublimation (PECSS) technique to improve the efficiency of CdTe PV devices. Specifically the DC hollow cathode plasma produced in the PECSS reactor was used to clean a substrate prior to deposition of the CdS window layer. The plasma cleaning process was found to nearly eliminate pinholes. In subsequent PV cell fabrication work by Swanson et al (2012b) the pre-deposition, plasma cleaning process enabled thinner CdS layers to be used, which increased the short circuit current, open circuit voltage, and cell efficiency. Finally Swanson (2012c) has shown that (1) operation of the PECSS device in O_2 during the deposition of CdS improves

transparency of the window layer by formation of oxygen doped CdS and (2) operation of the PECSS in N_2 during the deposition of CdTe improves carrier density by the formation of nitrogen doped CdTe. Successful nitrogen doping may reduce or eliminate the need for copper doping.

1.2 Research Focus

The use of a wire anode or a remote plate anode to produce plasma in heated pocket deposition (HPD)/close-spacing sublimation (CSS) geometries is unique, and this thesis presents measurements of plasma properties produced in the geometries introduced by Swanson et al (2012a,b,c). A diagram of the PECSS diagnostic source is shown in Figure 1-2. The PECSS diagnostic source measures 7.3 cm x 6.6 cm x 1.9 cm below the mesh with an additional 0.6 cm in height above the mesh and below the glass substrate.

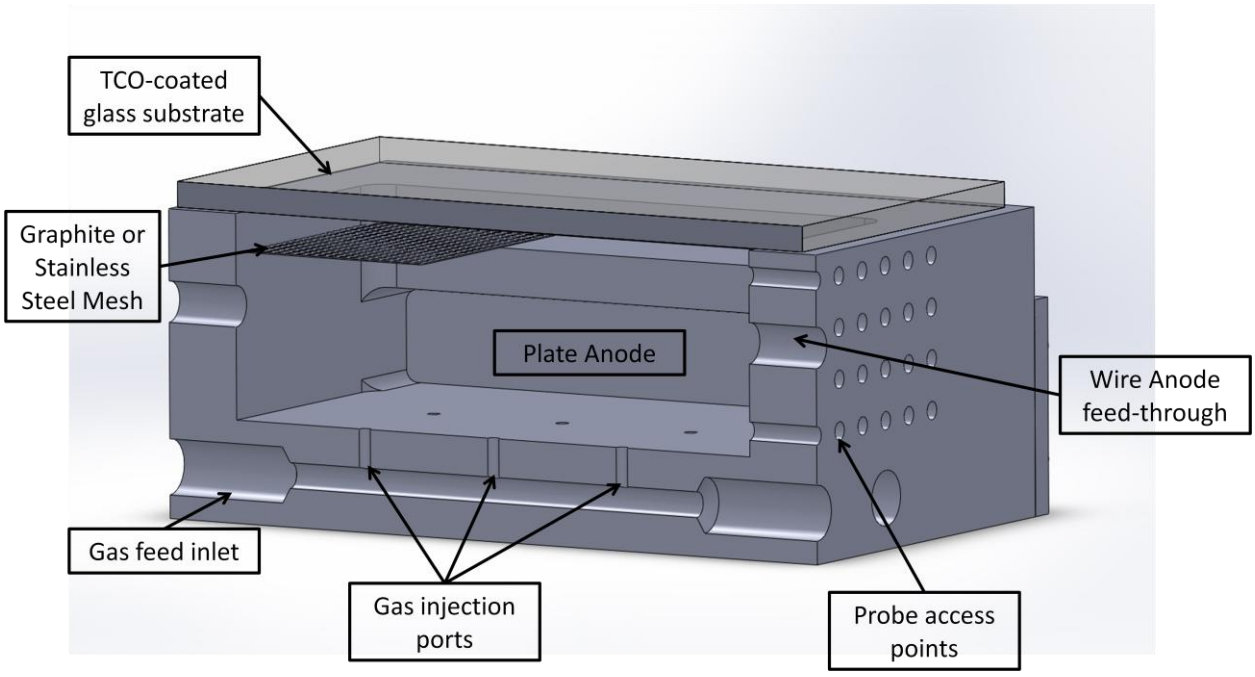

(a)

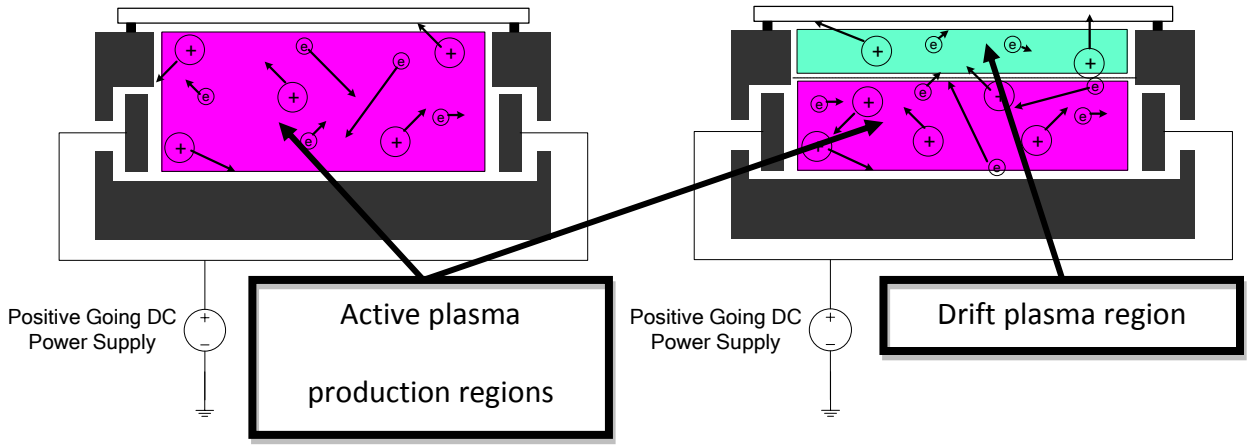

(bi) (bii)

Figure 1-2. (a) PECSS diagnostic source cutaway, (b) PECSS Diagram (i) without a mesh and (ii) with a mesh

The TCO-coated substrate, conductive side down, is placed on top of the PECSS device and electrically connected to the cathode. The TCO-coated glass is the surface on which the semiconductor material is deposited for the manufacture of CdS/CdTe PV devices. The mesh is placed in the source to separate the active plasma from the drift plasma and controls the intensity of the plasma next to the substrate. The mesh is cut away in Figure 1-2a for easier viewing of the source but it spans the entire pocket when in use. In Figure 1-2b the two configurations of the PECSS device are shown. With no mesh the TCO-coated substrate is part of the plasma production circuit. Fast moving ions strike the substrate along with the other cathode surfaces at high flux and emit secondary electrons, which sustain the discharge. With the mesh in place electrons in the drift region have low energy and do not contribute to significant plasma production. Plasma does exist here due to ions drifting from the active plasma region through the mesh. These ions can strike the surface of the substrate but with lower flux and lower energy compared to the operation without the mesh. This topic is further discussed in Section 3.5, where the ion current flux present at the TCO-coated surface is compared with and without the mesh in place. The gas feed inlet and injection ports allows for process gas to be fed through the bottom of the pocket and more evenly distributed through the PECSS device. The series of probe access points on the right side of the source allow for Langmuir probes (not shown) to be inserted into many locations of the pocket to adequately characterize the spatial properties of the plasma. The device shown, setup with plate anodes in Figure 1-2a, has the ability to also be run with a wire anode if desired using the wire anode feed through holes located on the side walls of the source.

To strike the plasma in the PECSS device, the pressure in the pocket is first brought to the desired range by feeding in the process gas. Next, the high voltage power supply, which is connected to the anode, is turned up until the required breakdown voltage is reached at which point a plasma will fill the pocket at which point the operating voltage will drop into the 300-500 V range. The remotely located plate anodes allow for the hollow cathode discharge to exist without the physical presence of a hot wire anode. This allows for more uniform treatment of a surface in processes like CdS/CdTe film growth that are sensitive to substrate temperature. In Section 3.6 data are presented on PECSS, with plate anodes, operating characteristics including discharge current and voltage with and without the mesh in different pressure ranges. Operating characteristics are also presented for a wire anode without the mesh for 7.3 cm x 6.6 cm x 1.9 cm geometry. Further the scaling of the PECSS technique was investigated using a 36.8 cm x 40.6 cm x 3.2 cm pocket with a thin wire anode run. The larger surface area allowed for operation at lower neutral compared to the smaller pocket. Operating characteristics of the larger source are also presented in Section 3.6.

To characterize the discharge present in the PECSS sources several electrostatic probes were used. Langmuir probes were used to measure properties in the plasma such as electron temperature, plasma density and plasma potential. The theory of Langmuir probes including the development of probes for this research is discussed in Section 2.3. Data were collected in both the discharge and drift regions of the PECSS diagnostic source and the results are compared in Section 3.2. An emissive probe was also used to verify the results of the Langmuir probe. Discussion of the emissive probe including probe construction and results are included in Section 3.3. A substrate with a segmented TCO-coated surface was used to measure the ion

current density strikes the glass as a function of position. Each segment was isolated from one another by laser scribe lines. Profiles of the ion current are plotted and discussed in Section 3.5 under varying pressure and power densities. The experimental ion current profiles were compared with a three-dimensional mathematical model of the PECSS reactor. Good agreement between the model and spatial trends in experimental measurements was observed.

As mentioned earlier, three-dimensional numerical modeling was performed on the PECSS reactor to calculate plasma production rates and transport processes. An earlier numerical model, as described by Makarov et al (2006), of a cylindrical cathode with a thin anode wire showed that high energy electrons (primaries) are the main driver of ionization, and our 3-d model of the more complicated PECSS geometry suggests that this is also true. Results obtained from our model are compared to experimental measurements in Section 4.3, and, although good agreement was found, our simple model would be improved if spatially varying EEDFs were used. One important finding uncovered in both experimental and modeling results is that the primary electrons emitted from the wall lead to high ionization rates in the corner of the source where four wall surfaces meet. The enhanced ionization rates in these regions help to offset strong diffusion losses that occur at these corners. These offsetting effects led unexpectedly to very uniform plasma over a majority of the source. Others have performed more elaborate numerical studies on hollow cathode geometries to determine properties such as the electron energy distribution function (EEDF) [Hashiguchi et al (1991)], electron densities, and potential profiles [Bogaerts et al (2002), Kutsai et al (2000)]. In future work presented in

section, it is recommended that these more elaborate models be adapted to the PECSS plasma source.

CHAPTER 2: MATERIALS AND METHODS

The focus of this chapter is on describing the PECSS device and the vacuum test facility. The diagnostic tools used to characterize plasma properties are also described.

2.1 PECSS device and setup

Two nearly transparent anode configurations were used to strike and maintain a discharge. They included a thin wire, approximately 0.254 mm in diameter, made out of tungsten, passed through the middle of the source cavity and plate anodes that were placed on opposing sides of the cavity as shown in Figure 1-2b. In the plasma cleaner configuration described by Swanson et al (2012a), the discharge is bounded by the graphite crucible at the sides and below and by the TCO-coated substrate above. In this configuration the TCO-coated substrate is an active component of the plasma production circuit (See Figure 1-2b (i)). In the PECSS geometry the discharge is bounded again by the graphite crucible at the sides and below, however it is bounded by a mesh above (See Figure 1-2b (ii)). In the PECSS geometry the TCO-coated substrate is not part of the plasma production circuit, but it is exposed to plasma that diffuses from the active region. Both plasma cleaning and PECSS configurations closely resemble the heated pocket deposition sources used for CdS/CdTe photovoltaic manufacturing at Colorado State University.

The discharge developed in the PECSS device exhibits several modes. Some of these modes are immediately useful for processing while require further investigation to be of use for PV cell processing. A diagram showing the approximate operational range over which different plasma modes occur is shown in Figure 2-1. Depictions of varying operating modes of the discharge are shown in Figure 2-2. The oscillating discharge occurs at very low discharge

currents. At this condition the voltage of the power supply increases until breakdown occurs, however the current is not high enough to maintain the discharge and it extinguishes. Next the voltage increases until breakdown occurs again. The oscillation frequencies were between ~5 and 50 hertz. In this oscillatory mode the visual glow of the discharge fills the entire pocket at the time the discharge strikes. The oscillation frequency increases as the discharge current is increased. The partial pocket, moving plasmoid operating regime the discharge does not fill the PECSS device and instead a plasmoid (globular plasma) is observed to slowly move around the pocket. At higher discharge currents the plasma transitions to a stationary plasmoid mode. The entire pocket is filled with plasma at neutral gas pressures above ~150 mTorr. The discharge is visually uniform and represents the mode most desirable for substrate cleaning and semiconductor deposition in this regard.

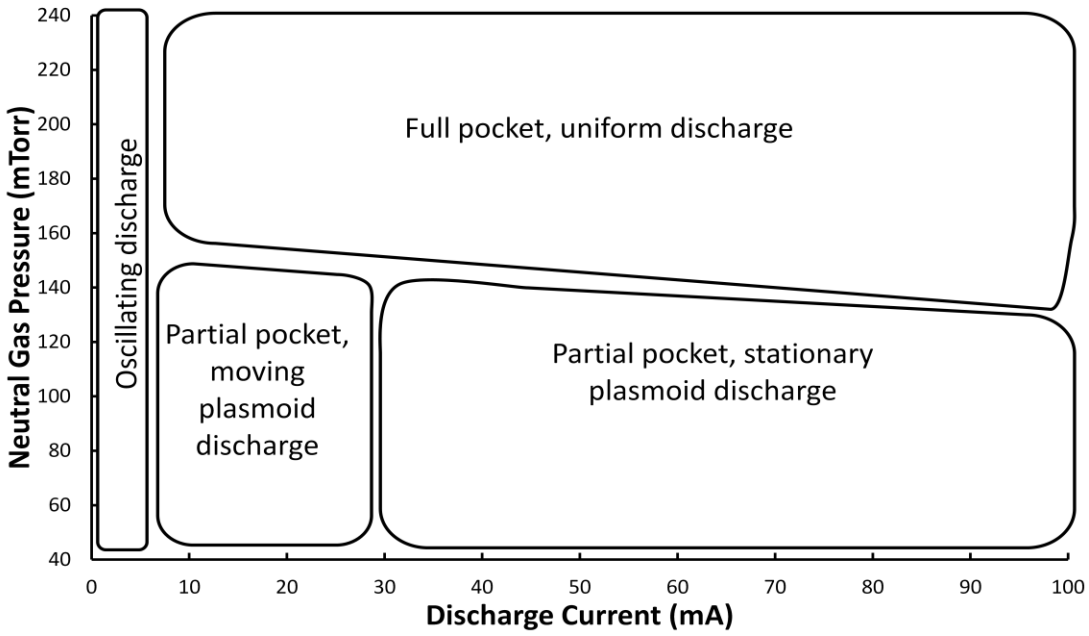

Figure 2-1. Approximate operating modes of plasma formed within a PECSS source. See Figure 2-2 for more information.

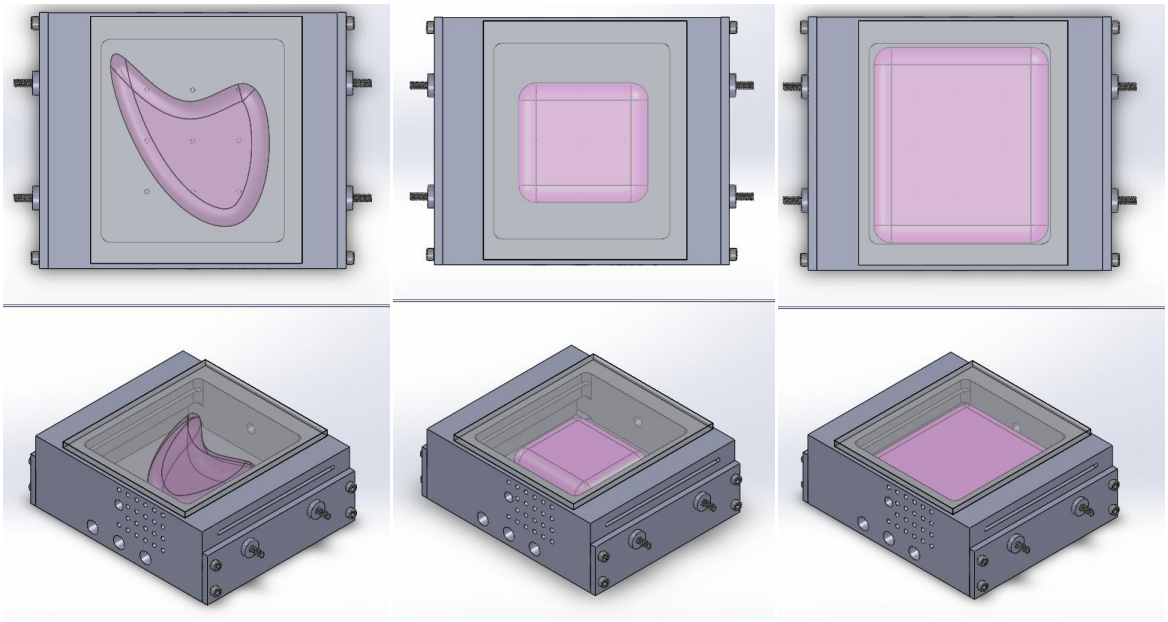

(a) (b) (c)

Figure 2-2. Operating modes of the PECSS device (a) partial pocket, moving plasmoid; (b) partial pocket, stationary plasmoid; (c) full pocket, uniform plasma discharge

2.2 Vacuum Facility

All tests on the 7.3 cm x 6.6 cm x 1.9 cm PECSS source were performed in a 0.64 m diameter by 0.76 m tall stainless steel bell jar evacuated by a mechanical roughing pump. The base pressure of the system was 10 mTorr without any gas introduced into the chamber. This pressure was obtained after 20 minutes of pump down time. The pocket pressure was raised to between 40-300 mTorr by flowing either 100% argon or a 98% nitrogen, 2% oxygen mixture of gas into the vacuum chamber.

2.3 Langmuir Probe

To characterize the plasma produced within the PECSS discharge, Langmuir probes were installed as shown in Figure 2-3. They were constructed using ceramic tubing and thin tungsten

wire. Photographs of the PECSS sources are shown in Figure 2-3b and c. The source in Figure 2-3c was designed such that probes could be placed in many locations to more thoroughly characterize the discharge. As described by C. Farnell (2007) a Langmuir probe consists of a conducting electrode that is placed in a plasma and biased to collect ion and electron current. Based on the current-voltage characteristics of the probe, discharge properties such as plasma density, electron temperature, and plasma potential can be determined [Farnell (2007), Beal (2004), Herman et al (2004a), Goebel (2005)]. A diagram of the Langmuir probe circuit used in this research is shown in Figure 2-3a.

A data acquisition system with both a voltmeter and ammeter was used with LabVIEW to record the current-voltage characteristics of the probe. A bipolar DC power supply capable of outputs between -100 and 100 volts and -4 to 4 A was used to sweep the probe. A typical current-voltage curve is shown in Figure 2-4.

There are several different regions in a Langmuir probe trace. Floating potential occurs when the electron and ion current collected at the probe are equal. At potentials that are significantly below floating potential (See Fig. 2-4), in the ion saturation region, electrons are repelled from the probe and mostly ions are collected. The voltage range between ion saturation region and plasma potential is known as the electron retarding region where both ions and electrons are collected to the probe. Above plasma potential no ions are collected to the probe and only electrons are collected. In a very dense, small Debye length plasma the current collected above plasma potential would not increase with increasing bias voltage, however, in most plasmas, as the voltage is increased, the electron collecting sheath becomes larger and more electron current is collected.

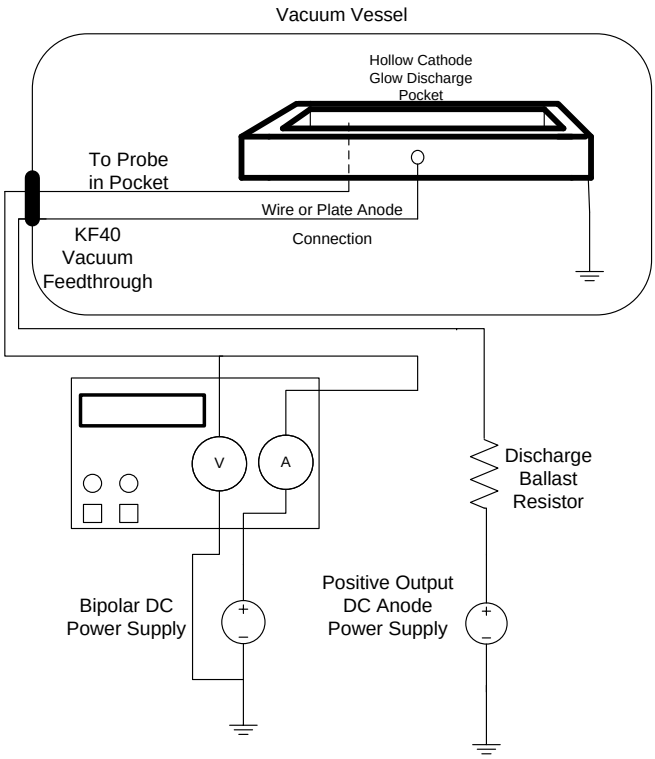

(a)

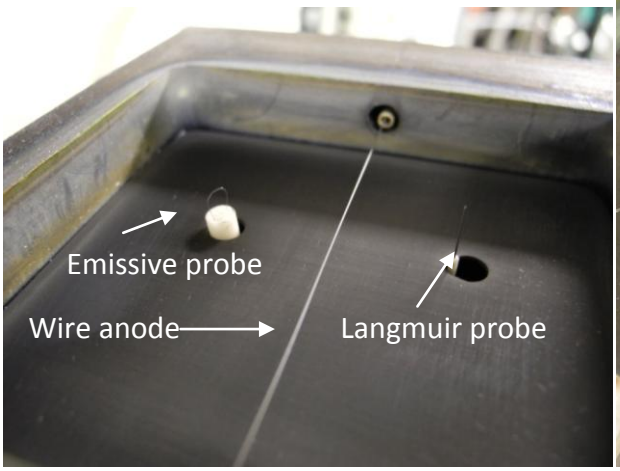

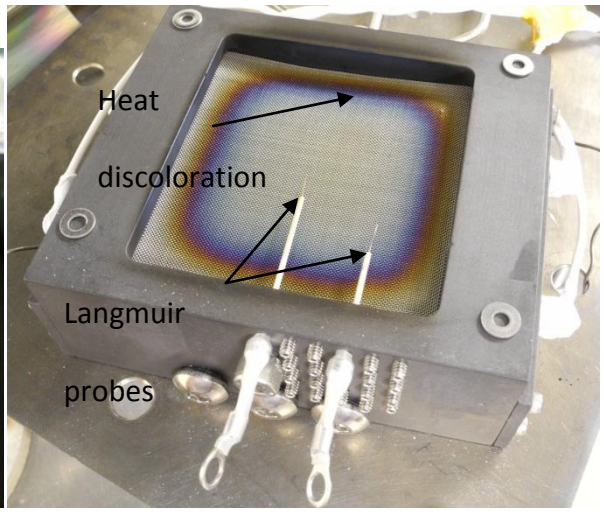

(b) (c)

Figure 2-3. (a) Langmuir probe circuit, (b) emissive and Langmuir probes in wire anode source, and (c) Langmuir probes in PECSS plate anode source

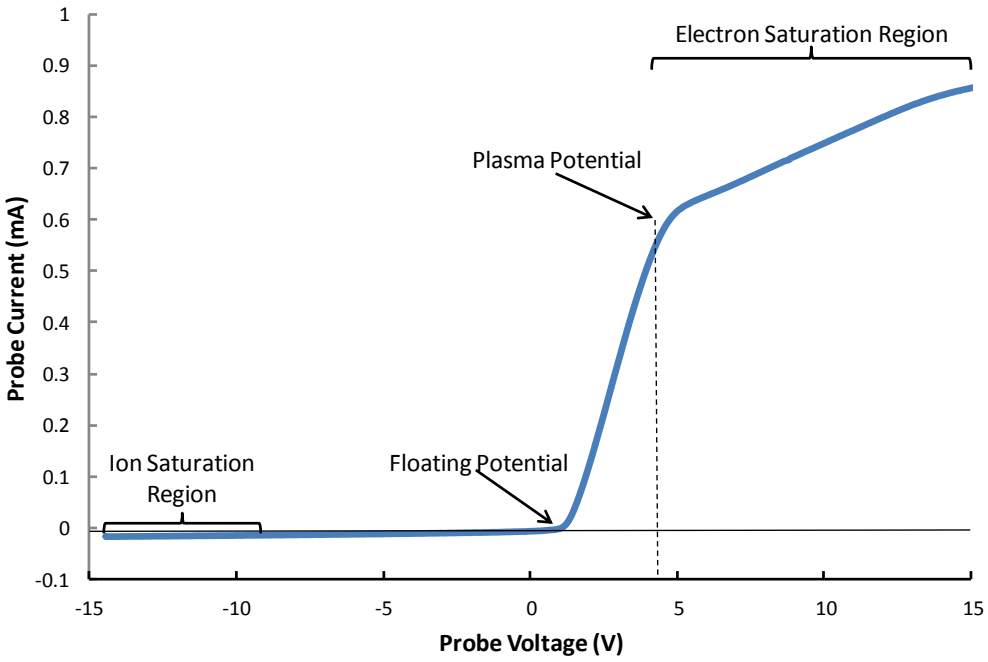

Figure 2-4. Typical current-voltage characteristics from Langmuir probe in PECSS device

Thin sheath analysis can be used when the probe radius is much less than the Debye length. The Debye length, λ_D, is given in Eq. (2-1). In the plasma produced in the PECSS geometries, the Debye length is comparable to the probe diameter so thick sheath analysis must be performed [Baldwin et al (2011)].

$$\lambda_D = \sqrt{\frac{\epsilon_0 * k_B * T_e}{e^2 * n_e}} \tag{2-1}$$

In the Eq. (2-1), ε_0 is the permittivity of free space, k_B is Boltzmann's constant, T_e is the electron temperature, e is the charge on an electron, and n_e is the plasma density.

When analyzing a Maxwellian electron distribution the electron temperature can be determined using Eq. (2-2) when fit to the curve in the electron retarding region after subtracting off the ion saturation current [Farnell (2007)].

$$\frac{k_B * T_e}{e} = \frac{1}{\frac{d \ln (I_p)}{dV_p}} \tag{2-2}$$

In Eq. (2-2), I_p is the probe current and V_p is the probe voltage. Once the electron temperature is known the plasma density can be found using equation 2-3.

$$n_e = \frac{4 * I_{sat,electron}}{e * A_{probe} * v_e} \tag{2-3}$$

In Eq. (2-3), $I_{sat,electron}$ is the current of measured at plasma potential, A_{probe} is the area of the Langmuir probe, and v_e is the thermal velocity of an electron. The thermal velocity of an electron is given in Eq. (2-4).

$$v_e = \sqrt{\frac{8 * e * T_e}{\pi * m_e}} \tag{2-4}$$

In Eq. (2-4), m_e is the mass of an electron. Sources of error can appear when taking and analyzing Langmuir probe data. The probe may perturb local plasma properties and there can be non-Maxwellian electrons within the plasma, such as primaries from cathode surfaces. Furthermore poor estimations of ion and electron saturation currents can lead to inaccurate calculations of electron temperature and plasma density. It is generally accepted that errors of ±25% exist in estimation of plasma density and errors of ±2V in plasma potential and ±0.2eV in electron temperature. Discussion of the Langmuir probe results are presented in Section 3.3.

2.4 Emissive Probe

Emissive probes have been used in a variety of plasma devices to measure plasma (or space) potential [Williams (1991), Herman et al (2004b), Smirnov et al (2004)]. An emissive probe was installed in the PECSS sources to measure the plasma potential and compare it to the one found using the Langmuir probe. When initially placed inside a plasma a surface will

float at a potential where the current of electrons and ions are equal. Surfaces will typically float a few volts negative of plasma potential to partially repulse the electrons, which have much higher mobility than the ions. A circuit diagram of the emissive probe is shown in Figure 2-5a, along with a photograph of the probe in Figure 2-5b.

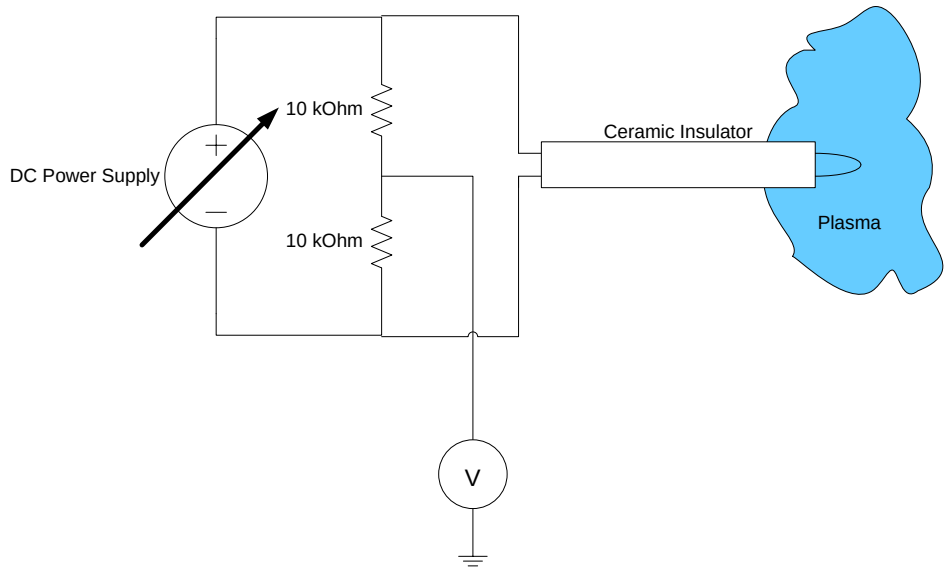

(a)

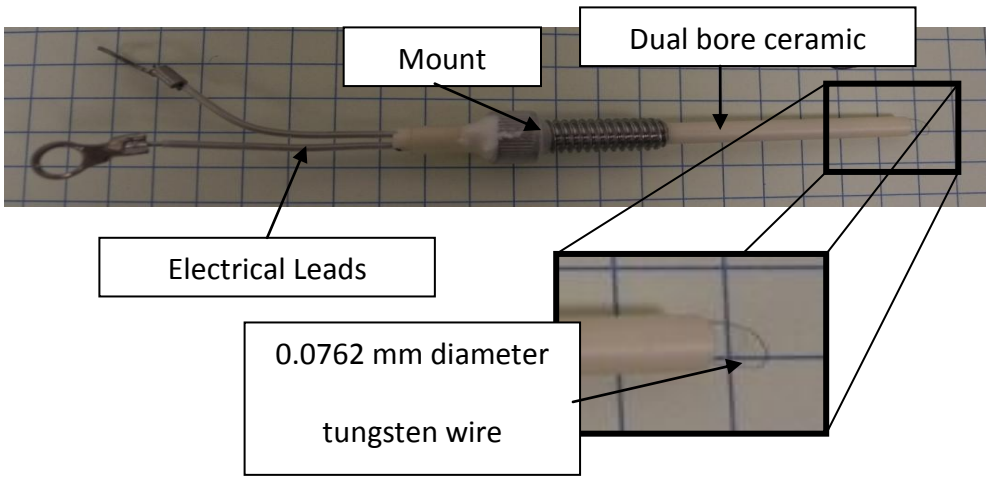

(b)

Figure 2-5. (a) Emissive probe circuit diagram and (b) emissive probe photograph

To create the emissive probe used in this research a hole was drilled through a socket head cap screw. A ceramic tube was then potted into the screw. The ceramic has two holes which accommodate 0.813 mm O.D. nickel capillary tubes in which a thin tungsten wire (0.0762 mm diameter) loop is crimped. Once the tungsten wire is crimped into the capillary tubing, the tubes are pulled back through the ceramic, leaving only the thin wire loop exposed. If the thin wire breaks due to overheating, the filament can be quickly replaced by crimping in a new filament. This process can be repeated until the nickel capillary tubing is too short to pass through the ceramic. A wire anode source with both emissive and Langmuir probes placed inside is shown in Figure 2-2b. Discussion of the emissive probe results are in 3.4.

2.5 Scribed Glass Probe

To determine the overall uniformity of the ion current striking the substrate, a TCO-coated surface was segmented using a laser scribe to create isolated, conductive, 5-mm-wide strips on the glass. Fourteen strips were created and were connected a resistor bank and then tied to cathode potential as shown in Figure 2-6. By measuring the voltage drop across each resistor, the ion current as a function of strip position was measured.

The ion current striking the surface cleans the TCO or modifies the semiconductor material being deposited on the substrate. Hence, measure of ion uniformity is important to document the expected treatment. Discussion of the ion current measurements to the TCO surface is contained in Section 3.5 of this thesis.

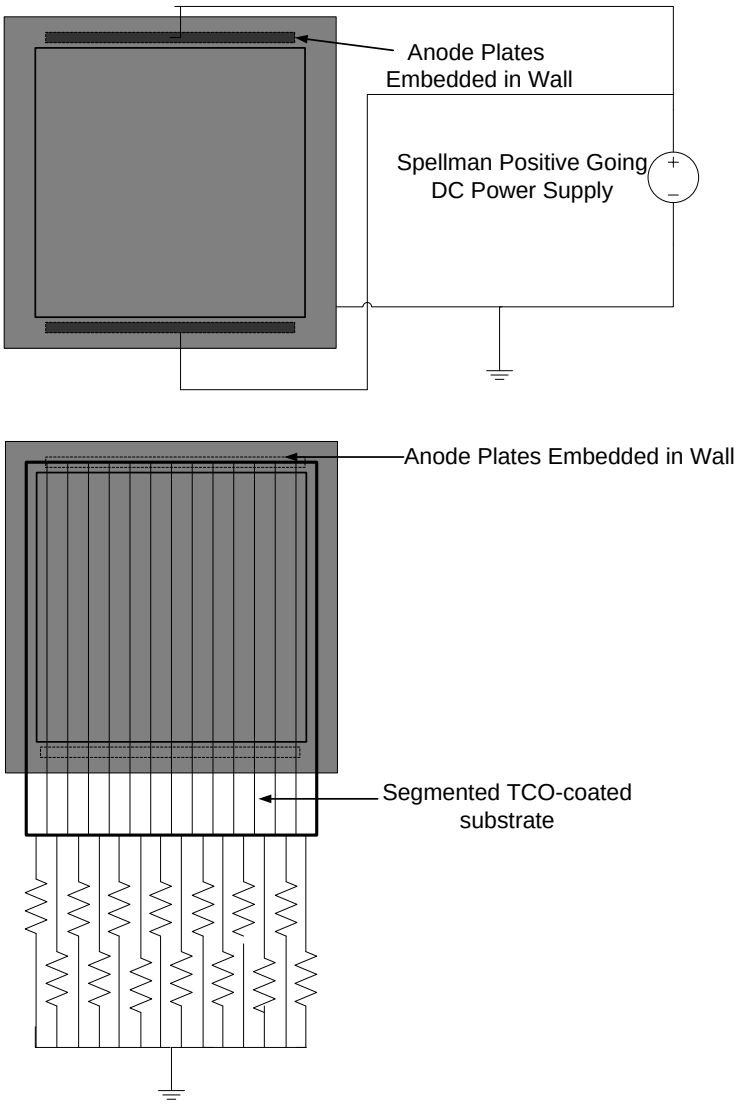

Figure 2-6. TCO- coated substrate wiring diagram on plate anode source

CHAPTER 3: RESULTS AND DISCUSSION

This chapter presents measurements of electron temperature, plasma density, and plasma potential obtained by Langmuir and emissive probes positioned in the active and drift plasma regions of the PECSS discharge. In addition, ion current profiles are presented, which document the uniformity of the plasma over the substrate.

3.1 Plasma Cleaner Geometry

When the PECSS device is used as a pre-deposition cleaner of a TCO-coated substrate, the substrate is in direct contact with the active plasma. A picture of the wire anode PECSS device being used as a pre-deposition cleaner is shown in Fig. 3-1. The substrate, which is held at cathode potential, can have one of several reactions occur when an ion strikes it. Ions striking the cathode surface deposit their kinetic energy into the surface liberating secondary electrons and sputtering cathode atoms. In addition plasma ions can implant into a surface and be incorporated interstitially or substitutionally into the material.

Swanson et al (2012a) used a Scanning White Light Interferometer (SWLI) to view CdS layers that were deposited onto TCO-coated substrates that were plasma cleaned. SWLI data are shown in Fig. 3-2 (a) and (b) for both the plasma cleaned and control substrates. When a substrate is cleaned using aqueous-based cleaning [Swanson et al (2012a)], pinholes appear in the CdS layer, which degrade the performance of solar cells by forming small shunting diodes between the TCO and CdTe films. The resulting pinhole formation is observed in Fig. 3-2(a) for the control substrate. Examination of the SWLI data presented in Fig. 3-2 (b) indicates that pre-deposition plasma cleaning of the substrate completely eliminated the pinholes in the CdS layer. Elimination of pinholes allowed for thinner layers of CdS to be used, which increased

light transmission to the CdTe layer in a full device formed from the plasma cleaned surfaces. With the thinning and the elimination of pinholes; the PV cell efficiency, fill factor, and short circuit current increased. The pre-deposition plasma treatment used by Swanson et al (2012a) with operating conditions of 200 mTorr nitrogen/oxygen (98%/2%), 30 mA, is characterized in this thesis along with many other similar operating conditions.

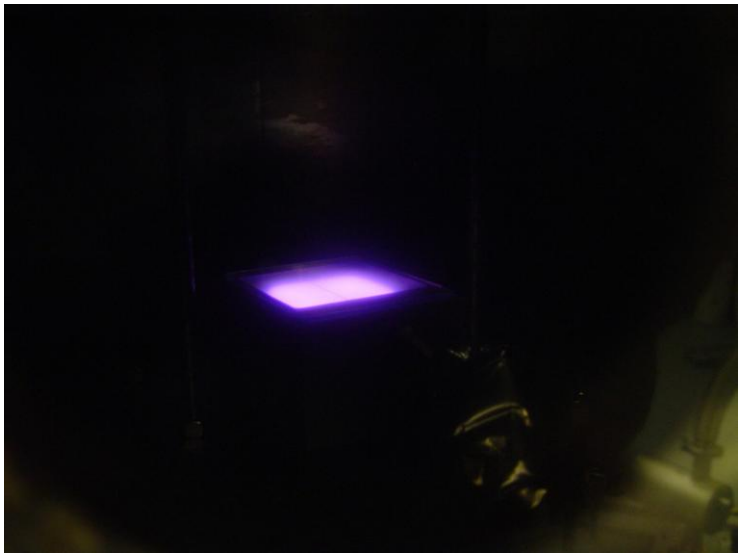

Figure 3-1. Wire anode PECSS device running as a pre-deposition cleaner.

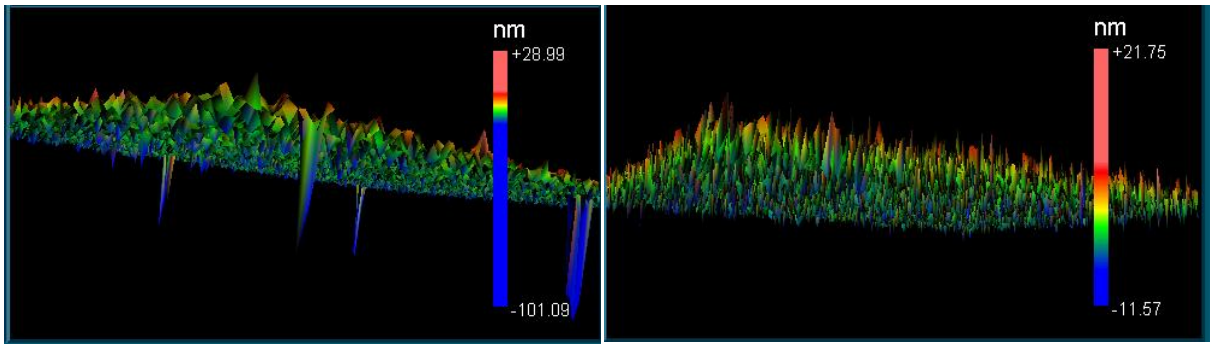

(a) (b)

Figure 3-2. (a) SWLI data showing pinholes present in the CdS after standard cleaning of the substrate, (b) SWLI data showing the CdS layer created after pre-deposition plasma cleaning [Swanson (2012c)].

3.2 Deposition Mode Geometry

In addition to cleaning, plasmas can be helpful when depositing films within heated pocket deposition sources. In deposition mode, the glass, still held at cathode potential, is separated from the active plasma production region by a mesh and drift plasma region as described in Sections 1.2 and 2.1. This allows ions to drift through the mesh and strike the TCO-coated substrate at lower flux levels and with improved uniformity.

3.3 Langmuir Probe Results

Plasma density and electron temperature data measured with a Langmuir probe positioned in the active discharge region are shown in Fig. 3-3. As the discharge current is increased the Maxwellian electron temperature decreases from 5 eV to 1 eV. The plasma density increases with increasing discharge current because (1) the ion current density flux to the wall is directly proportional to the discharge current, (2) the electron temperature is relatively constant, and (3) the ion flux is directly proportional to plasma density. It is noted that the electron temperature and density are too low to sustain the ion production rate in the PECSS discharge. Instead, it is believed that primary electrons are mostly responsible for ion production in the discharge, which is supported by numerical modeling as discussed in Chapter 4 of this thesis.

Langmuir probe results from the drift region of the PECSS device are shown in Fig. 3-4. In this region the plasma densities are similar to those in the discharge region, for the same discharge current settings. In addition, the electron temperatures are a factor of 10 to 15 times lower than those measured in the discharge region.

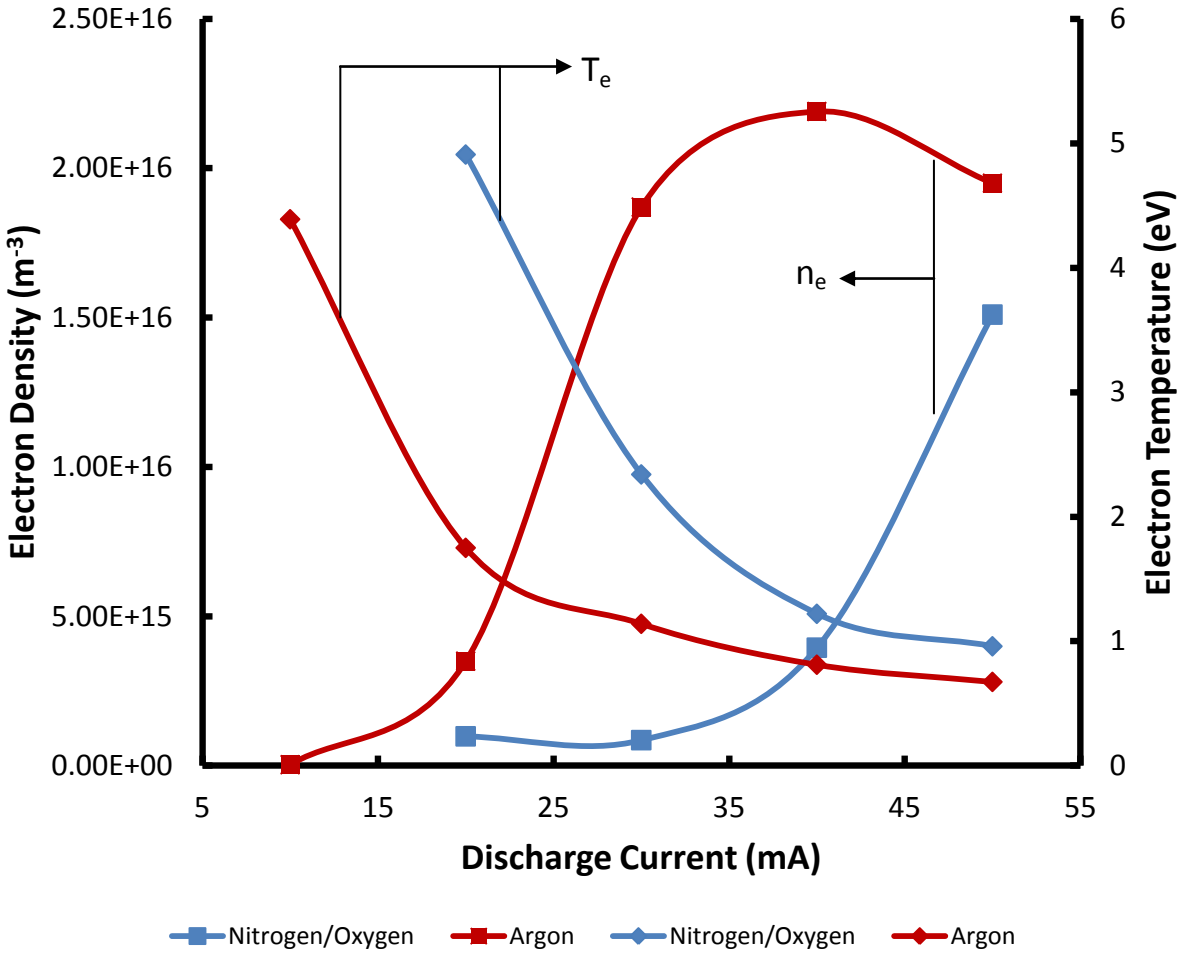

Figure 3-3. Langmuir probe results in the active discharge region of PECSS, plate anode source, 200 mTorr N_2/O_2 (98%/2%) and argon.

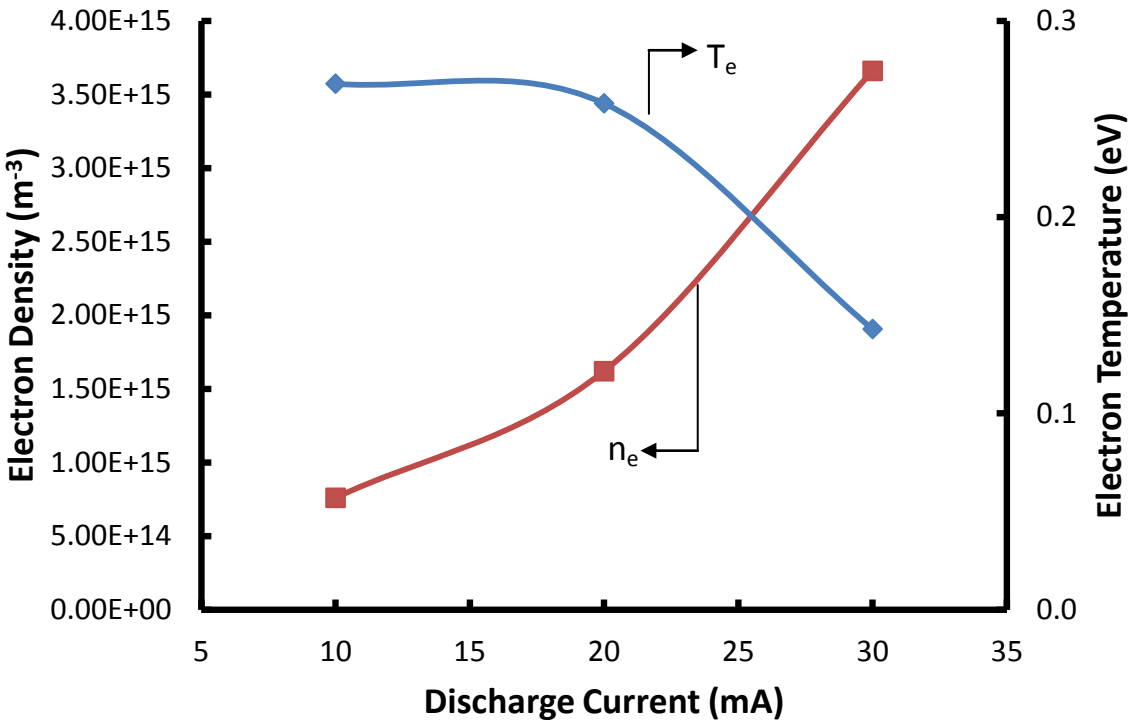

Figure 3-4. Langmuir probe results taken in drift region of PECSS, plate anode source, 200 mTorr N_2/O_2 (98%/2%). See Fig. 3-3 to compare to active region data.

The plasma potentials which are measured with the Langmuir probe in the active discharge region typically are a few volts negative of anode potential. The plasma potential does not vary greatly when the discharge current is varied. One very important finding, however, was that the plasma potential in the drift region of the PECSS device was only a few volts above cathode potential. This result suggests that ions would be accelerated from the active region into the drift region where they would impact the substrate during film growth. These energetic ions would assist the film by adding energy and allowing atoms to move and fill defect sites.

3.4 Emissive Probe Results

An emissive probe was used to measure plasma potential in both the active discharge region and drift plasma region. This probe was used to confirm measurements of plasma potential made with the Langmuir probe. Emissive probe results are shown in Fig. 3-5 in a plot of probe floating potential versus filament heating current. At heating currents above 1 A, the floating potential saturated at a value very close to anode potential. Typically, plasma potential is near the anode potential, which holds true for both the Langmuir and emissive probe data presented in this thesis when the probes are positioned in the active discharge region and when the full pocket, uniform plasma operating condition was established.

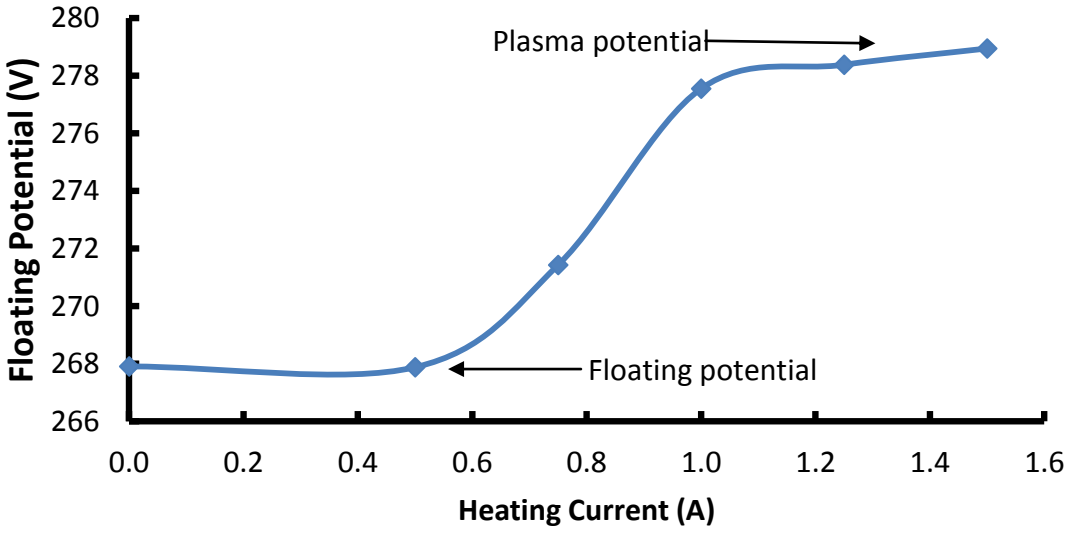

Figure 3-5. Emissive probe data collected within the wire anode PECSS device.

The floating potential and plasma potential of the drift plasma are shown in Fig. 3-6 measured with the emissive probe at several discharge current conditions. The plasma potential in the drift region is close to cathode potential confirming the interesting result

obtained with the Langmuir probe. Floating potential, which occurs when the filament current is zero, varies by a few volts over a discharge current range of 10 mA to 50 mA. As the discharge current is increased from 10 to 50 mA the plasma potential in the drift plasma increases from ~3-7 V. The ions which are present in the drift region are generated in the active plasma region below the mesh. In deposition mode the passing through the drift region can be incorporated into the semiconductor film and assist the deposition in other ways as mentioned earlier.

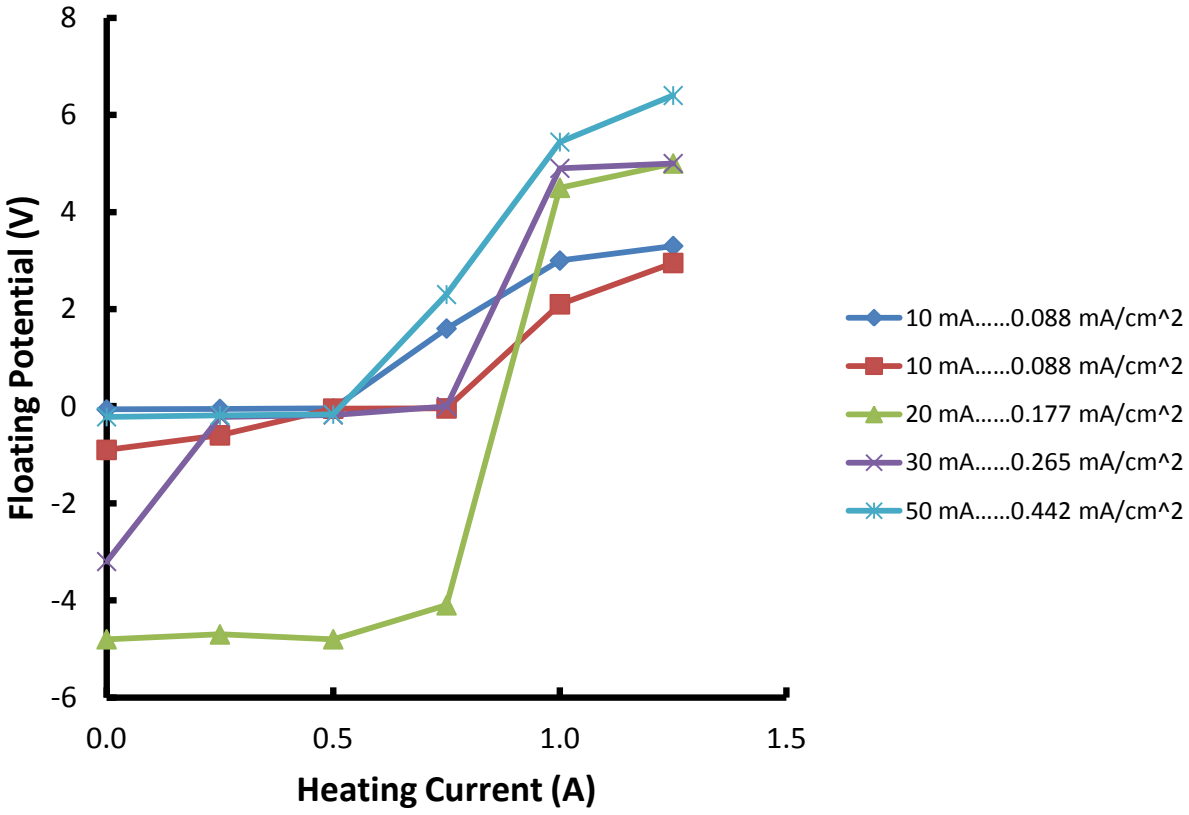

Figure 3-6. Emissive probe results obtained in drift plasma.

3.5 Segmented Glass Results

A TCO-coated glass substrate was segmented into isolated 5 mm wide by 65 mm long strips using a laser scribe. The scribed TCO glass was then placed over the PECSS device and the ion current striking the strips was measured for several discharge currents and neutral gas pressures. Figure 3-7 shows the ion current to the TCO strips at as a function of strip position. When there is no mesh in place, the ion current profiles have two peaks that move toward the wall as the pressure is increased. These peaks occur at about two ionization free paths (of the primary electrons) from the graphite side walls. The mean free path of a primary electron decreases as the pressure is increased, and this is believed to be the reason why the strip current peaks move toward the wall as pressure is increased. The ionization rates in the regions of intersections between top, bottom, and side walls are believed to be higher compared to the centerline regions where only two walls (top and bottom) are nearby. The beam of primary electrons that flows off of a wall results in an initial primary electron concentration that drops off as a function of distance from the wall. The primary electron concentrations add from each wall and are higher in corner regions. Ion production rates are proportional to the primary electron concentration and neutral gas density, and strip ion current is proportional to ion production rates directly above the strip. Hence one would expect the strip ion current to peak on each side of the discharge where ionization rates and primary electron concentrations are higher.

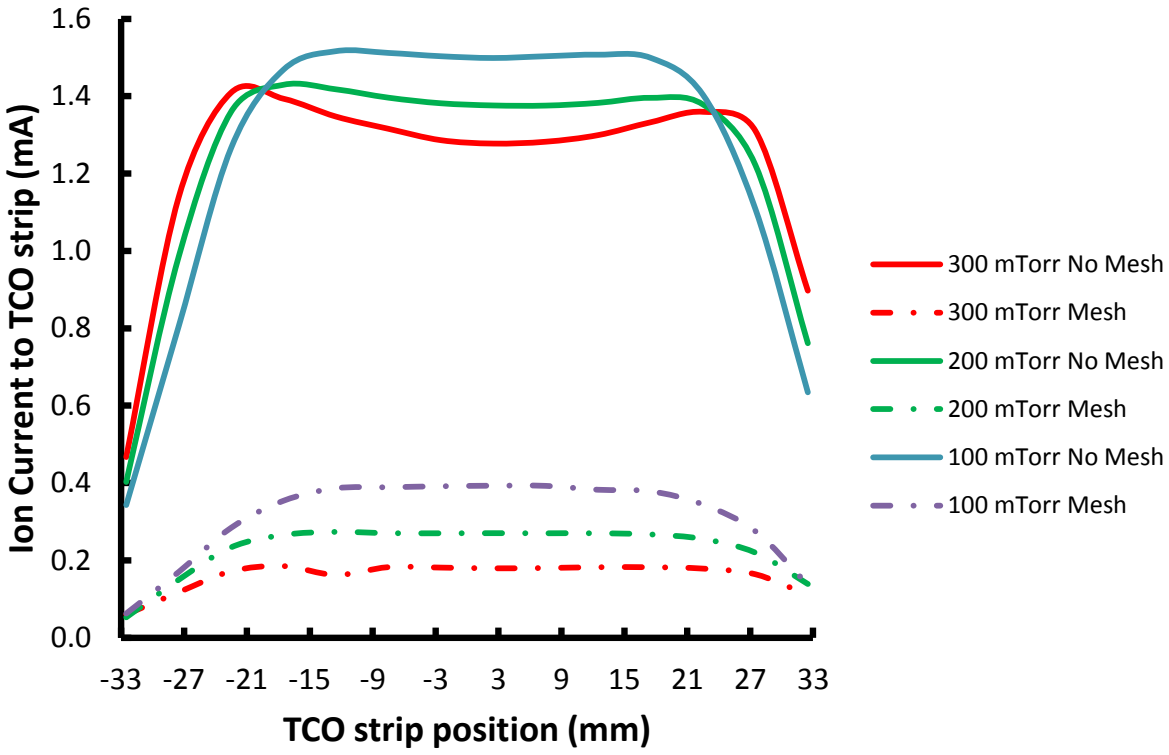

Figure 3-7. Strip ion current to the substrate with scribe lines oriented perpendicular to graphite walls where the anode plates were installed. Data are shown with and without the mesh present in a N_2/O_2 (98/2%) gas mixture and with a 50 mA discharge current.

Figure 3-8 shows similar results to those in Fig. 3-7; however these data were collected with the TCO strips oriented parallel to the walls where the anode plates were installed instead of perpendicular to them. The ion current to the strips near the centerline is higher compared to when the strips are oriented perpendicular to the anode plates due to the fact that no secondary electrons are produced at the anode plates. The ion current profiles shown in Fig. 3-7 and Fig. 3-8 are similar for all discharges that operate in the uniform, full pocket operating mode.

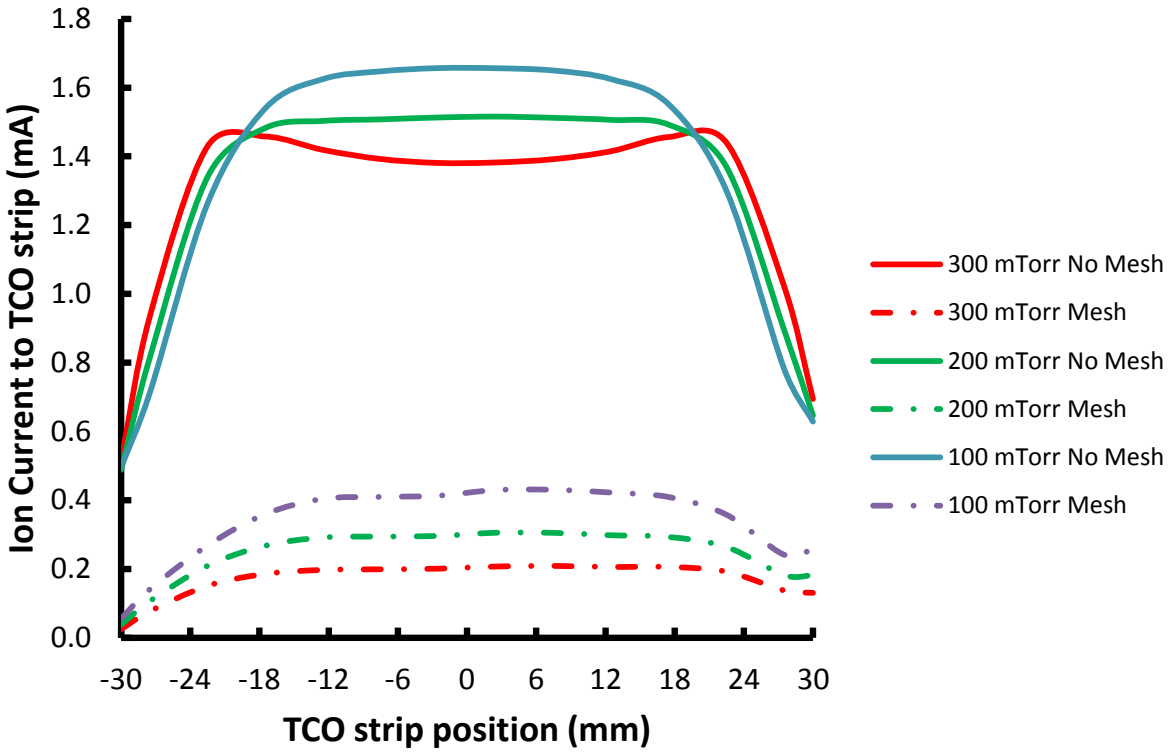

Figure 3-8. Ion current resolved at substrate with scribe lines parallel to plate anodes with and without the mesh in N_2/O_2 (98/2%) mixture at 50 mA discharge current.

When a mesh is placed in the PECSS device the strip ion current at the TCO glass surface decreases the ion current by a factor of 5-10. In addition, when the mesh is in place, the ion strip current is more uniform than without the mesh in place. The percentage of total ion current to the TCO relative to the discharge current with and without a mesh is shown in Fig. 3-9.

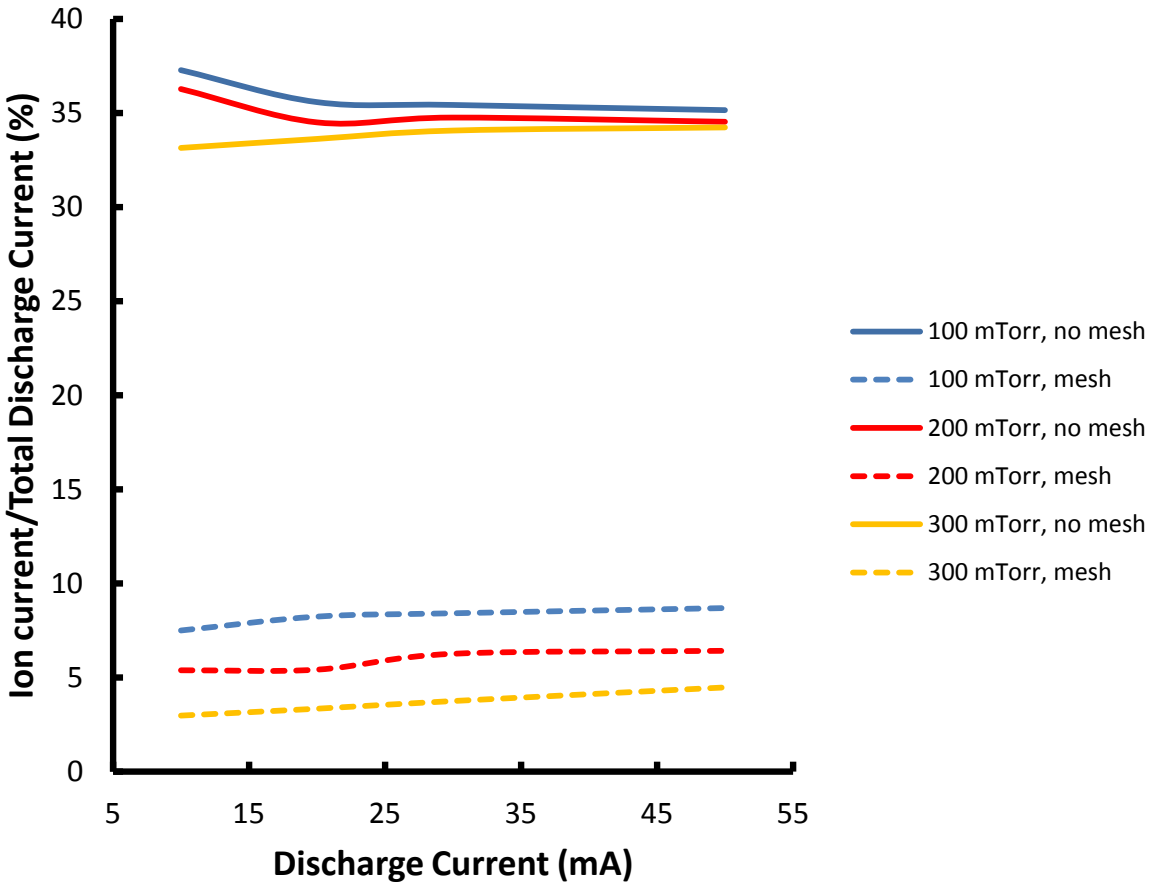

Figure 3-9. Percent of discharge current which strikes the TCO-coated substrate, comparing with and without a mesh in a N_2/O_2 (98/2%) mixture at neutral gas pressures ranging from 100-300 mTorr.

As seen in Fig. 3-7, Fig. 3-8, and Fig. 3-9 it is clear that the ion current is significantly attenuated when the mesh is used. This attenuation decreases the amount of energy deposited into the substrate. The open area of the mesh could be increased or decreased to allow for more or less attenuation, however, if the mesh open area or hole size gets too large, the drift region can become part of the active region, which may be undesirable for achieving the material processing that is required. In the PECSS device the fraction of the discharge

current reaching the TCO remains the same regardless of discharge current changes. The neutral gas pressure plays a more significant role in the fraction of discharge current which reaches the TCO. When no mesh is in place the fraction of discharge current reaching the TCO, about 35%, is fairly stable regardless of neutral gas density. When the mesh is in place, the affect between the neutral gas densities is more pronounced. As the neutral gas density is increased, the ions, which drift from the active plasma region, have an increasing number of collisions. Note that whether or not a mesh is used the lower the neutral gas density in the PECSS device the larger fraction of discharge current reaches the TCO.

In Fig. 3-10 the ion current to the TCO strips is plotted when the non-uniform, moving plasmoid operating mode was present. The operating mode shown in Fig. 3-10 is not only visually non-uniform but also non-uniform in the ion current profiles to the TCO-coated substrate. This operating mode is not ideal for pre-deposition plasma cleaning or deposition as the treatment of the substrate would be very non-uniform.

3.6 Current-voltage Characteristics

The current-voltage characteristics for both the 7.3 cm x 6.6 cm x 1.9 cm and 36.8 cm x 40.6 cm x 3.2 cm wire anode sources are shown in Fig. 3-11 and Fig. 3-12. The discharge voltages for the larger wire anode source are approximately 50 volts lower than those of the smaller anode plate source. Both the wire and plate anodes used in the smaller source show similar current voltage characteristics where the wire anode discharges were ~50 V lower than the anode plate discharges.

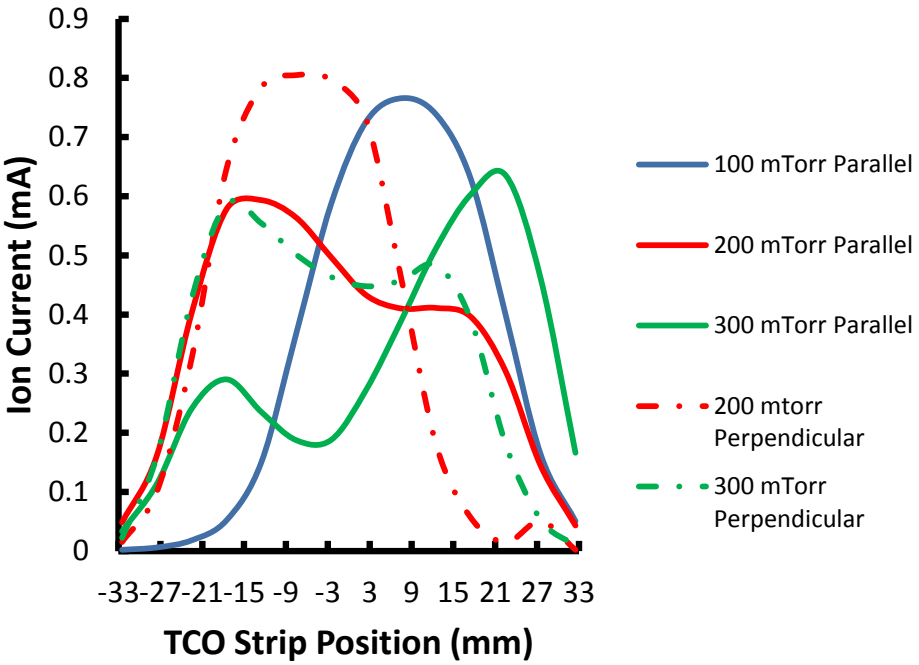

Figure 3-10. Ion current resolved at substrate when a moving plasmoid operation mode is present. [N_2/O_2 (98/2%) gas mixture, 10 mA discharge current].

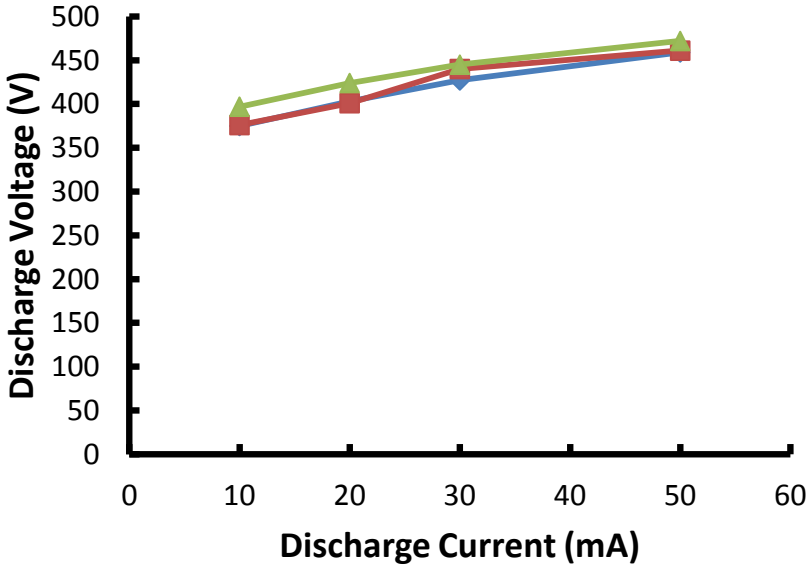

Figure 3-11. Current-voltage characteristics of PECSS device equipped with plate anodes that was operated with a 98%, 2% N_2/O_2 gas mixture.

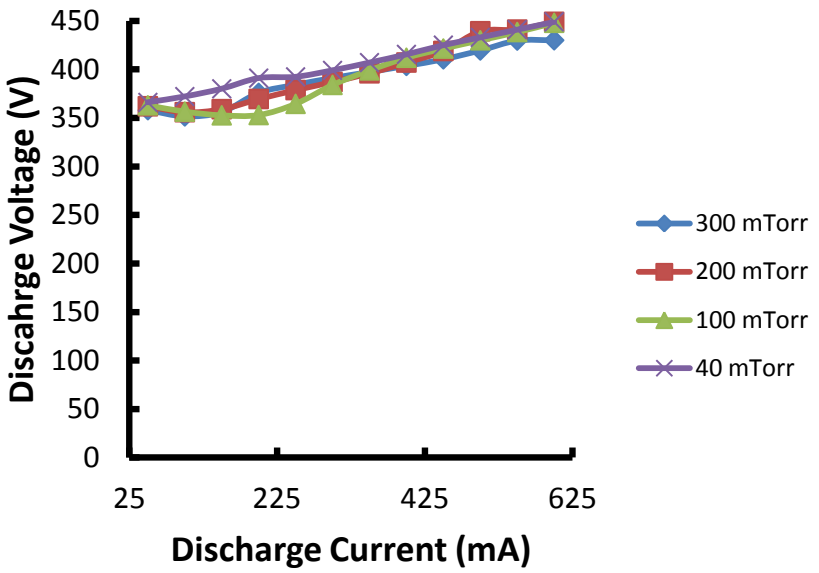

Figure 3-12. Current-voltage characteristics of the larger 36.8 cm x 40.6 cm x 3.2 cm wire anode source operated on a 98%, 2% N_2/O_2 gas mixture. Note that the discharge current values are higher and scale with cathode area.

3.7 Oscillating Discharge Mode

In the oscillating plasma mode the discharge current is set at a low value where the power supply cannot maintain a stable discharge. In this mode the power supply will increase in voltage until the required break down voltage is reached. This ramp up in discharge voltage occurs every time the plasma extinguishes. In Fig. 3-13 an oscilloscope was utilized to measure the discharge current and voltage of the PECSS device when it was operating in an oscillatory mode. The voltages range from ~375 to 550 volts. When the power supply reaches the required breakdown voltage the plasma discharge strikes and is followed by an increase in discharge current. Since the discharge current in the period after the discharge strikes is too low to maintain the plasma, the plasma extinguishes. Then the power supply starts to increase

voltage until breakdown occurs again. This process was observed over a range of low discharge currents. Visually, the plasma appeared to fill the entire PECSS device immediately after the breakdown voltage was exceeded.

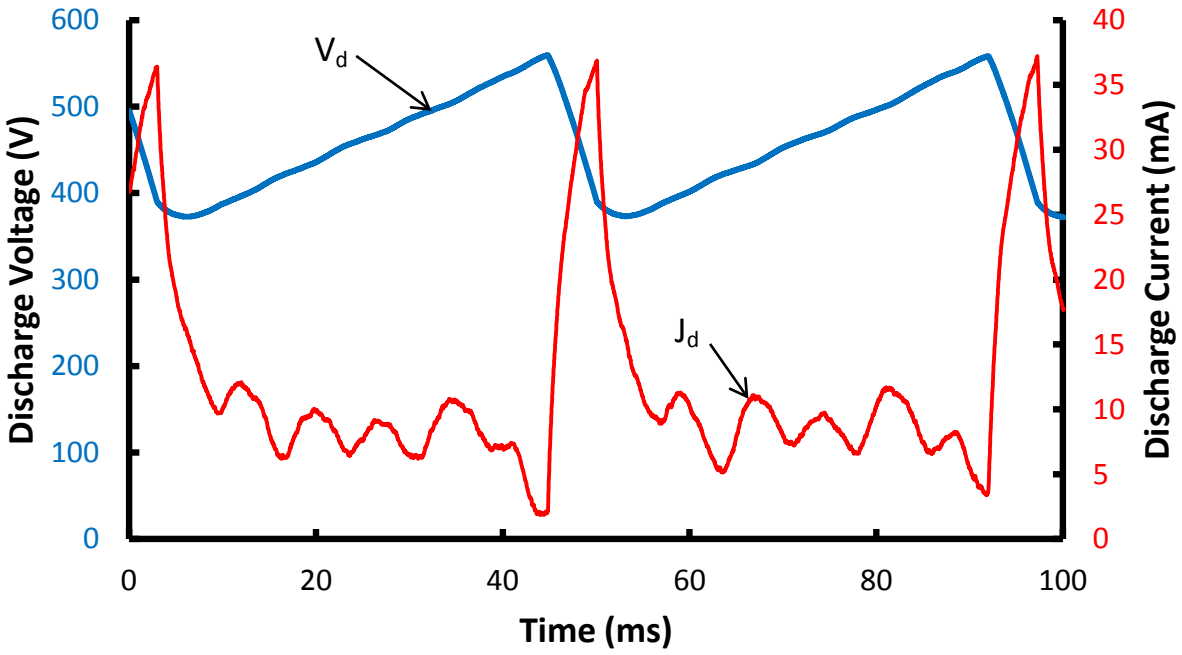

Figure 3-13. Oscilloscope reading of current and voltage characteristics when oscillating plasma is present.

Fig. 3-14 shows the measured breakdown voltages compared to the predicted Paschen curve breakdown voltages [Lisovskiy et al (2000)]. The voltages that were observed in the oscillating discharge in PECSS do not match the Paschen curve predicted values when the product of pressure (P) and discharge chamber height (d) was less than 0.1 Torr-cm. This may be due to the fact that the plasma present in the PECSS device may not completely extinguish before the power supply voltage increases and reignites the discharge. It is noted that the discharge chamber height, d, used to calculate "P d" was 1 cm. This is the distance from the

wire anode to the top of the chamber. It is possible that the distance from the wire anode to the side wall (3 cm) might also represent a good choice for d, which would shift the 0.04 and 0.075 Torr-cm points to the right where they would be closer to the Paschen curve.

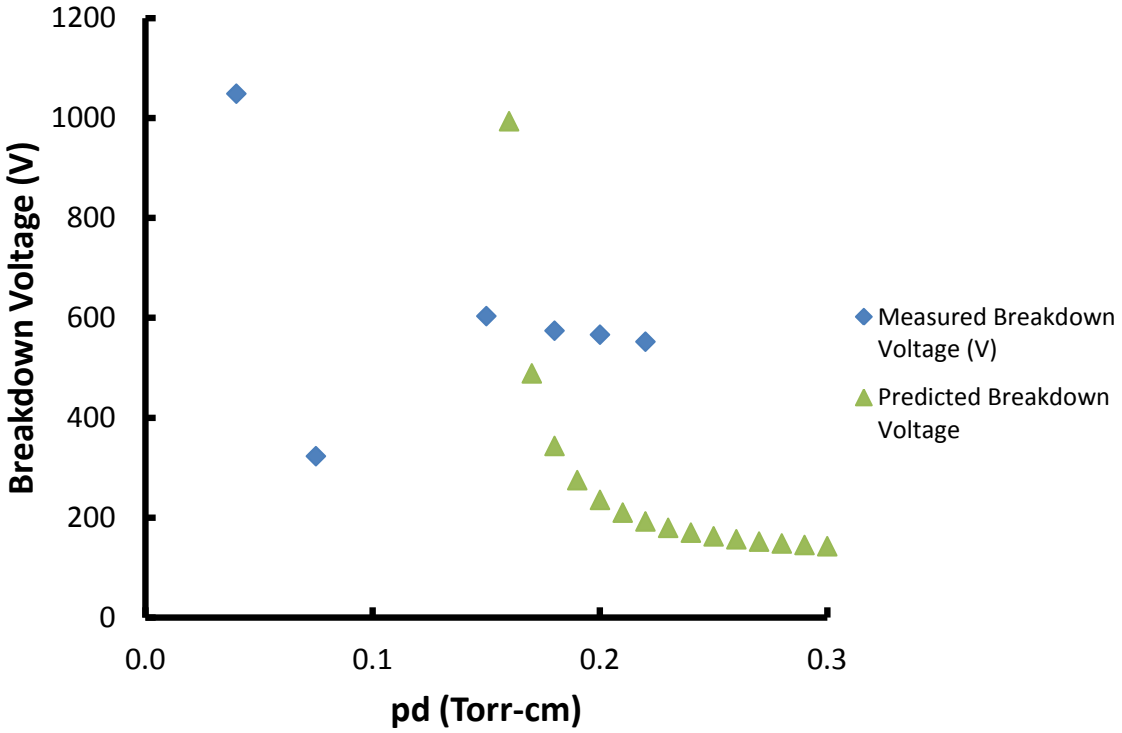

Figure 3-14. Measured breakdown voltages in PECSS device (blue) compared to expected breakdown curves.

3.8 Floating Substrate Experiment

Photographs of the drift plasma when no cathode walls are present in the drift region are shown in Fig. 3-15. Although the substrate is typically held at cathode potential when deposition is occurring, the carrier on which the substrate is placed may be insulated in future work allowing the substrate to electrically float. An experiment was performed to determine the floating potential of the TCO-coated substrate as a function of distance and discharge

current. The results of this experiment are shown in Fig. 3-16, 3-17, and 3-18. At low pressures (<75 mTorr) the floating potential decreases dramatically as the glass distance from the mesh is increased. As much as 250 V of floating potential difference is seen as the glass moves from 5 mm to 30 mm. Both the discharge current and current density of ions to the mesh are listed in the legend. The nominal distance between the mesh and the substrate during film deposition is set to ~6mm. At this spacing, an insulated substrate would float close to plasma potential and ions would strike the substrate at very low energies. This is opposite to the condition when the substrate is grounded. In this case the ions will strike at higher energies and could ion assist the deposition of the film. Both the grounded and floating configurations could be used to find optimum film growth plasma assisted operating points.

Figure 3-15. Photographs of the drift region as viewed with no cathode walls and a floating substrate.

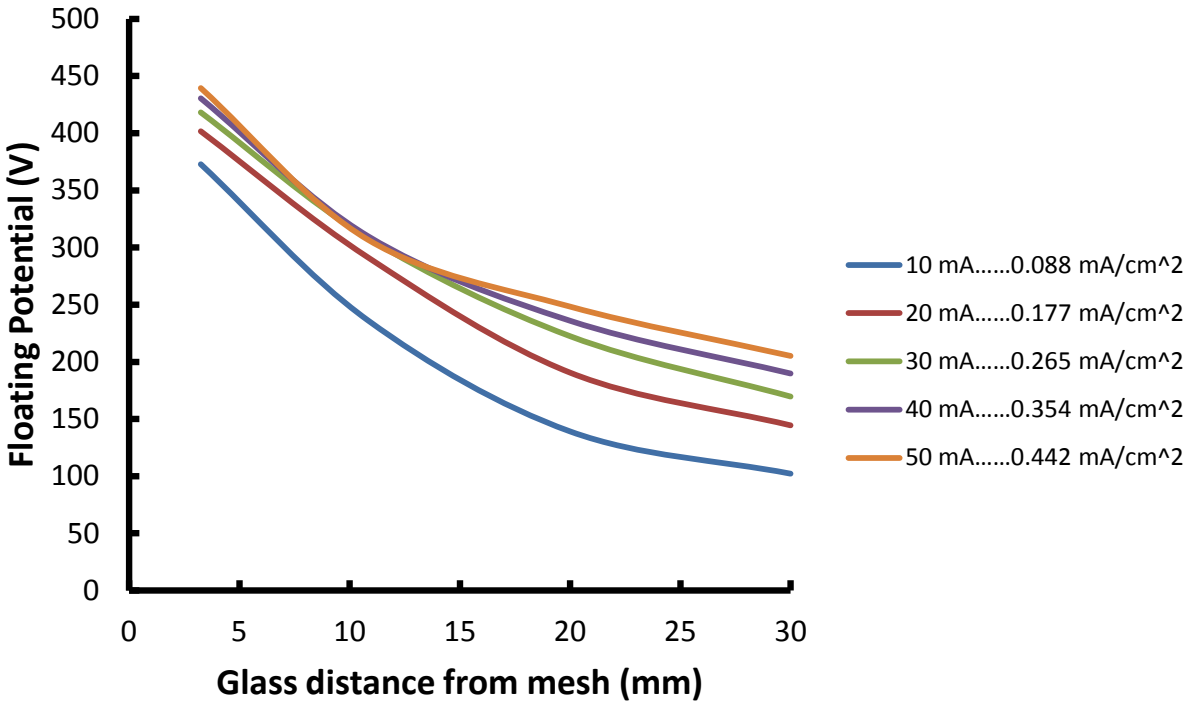

Figure 3-16. Floating potential of TCO-coated substrate at 50 mTorr N_2/O_2 (98%/2%).

Figure 3-17 shows the floating potential of the TCO-coated substrate at a pressure of 200 mTorr. Floating potential holds this trend for pressures between 100 and 300 mTorr. The floating potential falls slightly as the distance from the top of the mesh and the floating TCO substrate is increased. As the glass distance or neutral gas density is increased the number of collisions that a drifting ion has will increase and the energy with which the ion strikes the glass will drop.

Figure 3-18 again shows the floating potential but at a much higher pressure of 500 mTorr. At this pressure the floating potential is significantly lower than in the pressure range of 100-300 mTorr. While the floating potential in the 100-300 mTorr range is near that of the discharge voltage, in the 500 mTorr range it is ~300 V lower. Hence changes to both pressure and floating-grounding the TCO substrate will affect plasma ion assist during film growth.

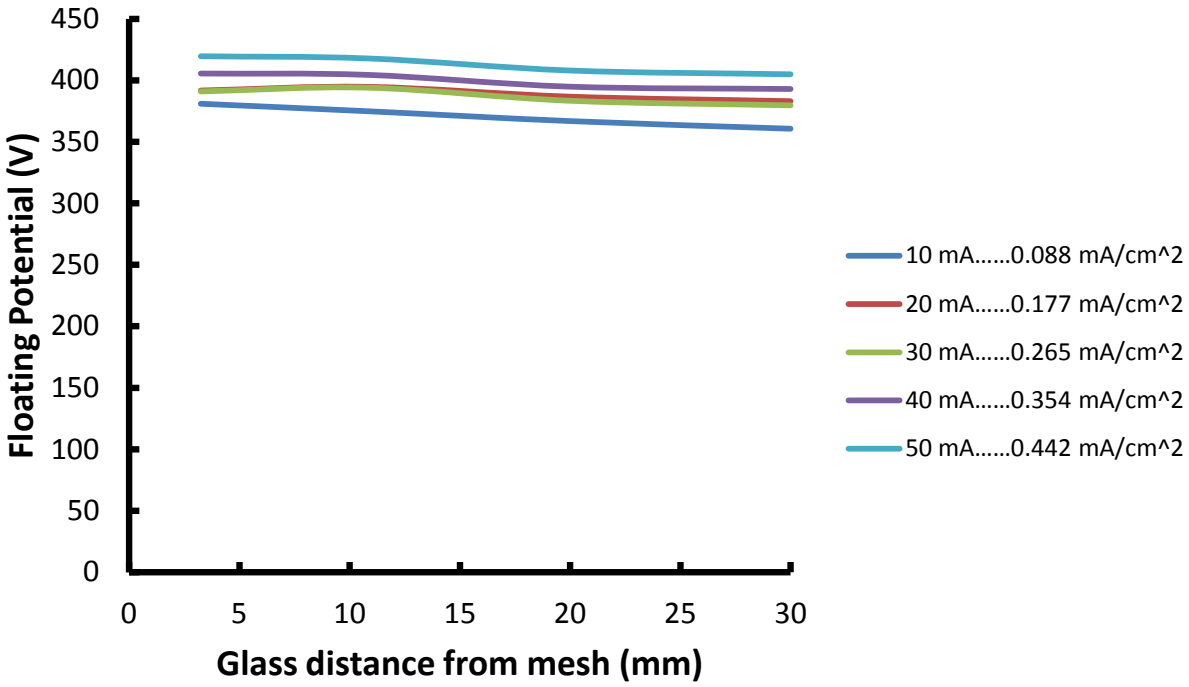

Figure 3-17. Floating potential of TCO-coated substrate at 200 mTorr N_2/O_2 (98%/2%).

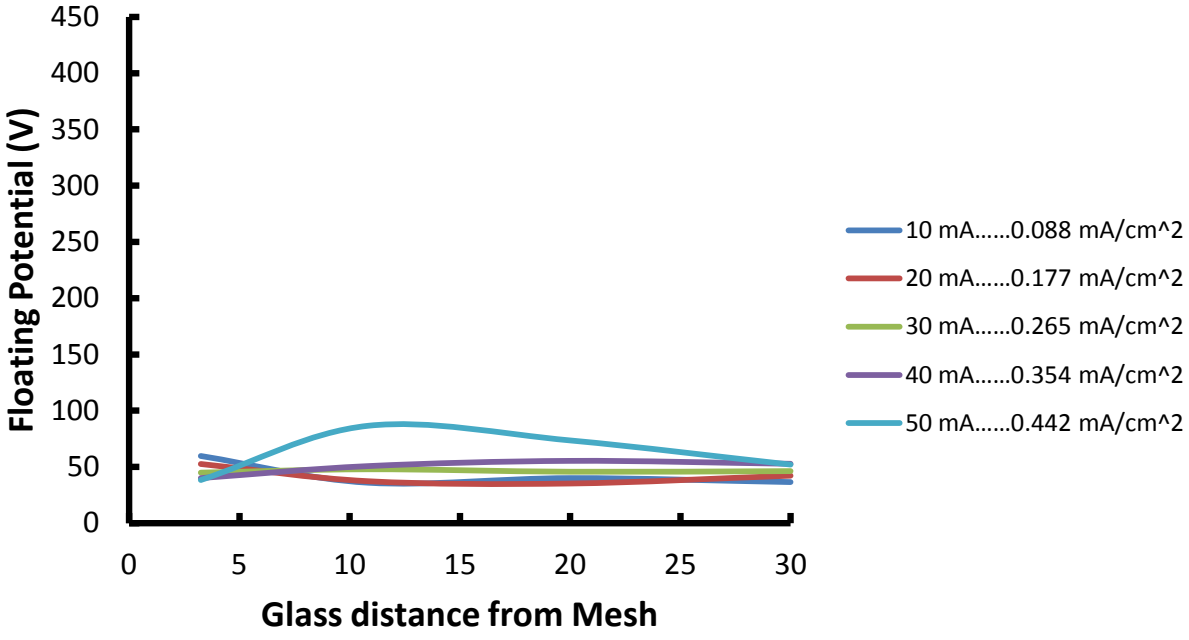

Figure 3-18. Floating potential of TCO-coated substrate at 500 mTorr N_2/O_2 (98%/2%).

CHAPTER 4: AMBIPOLAR DIFFUSION MODELING AND RESULTS

An ambipolar diffusion-based model was developed to model the active region of the PECSS discharge. This was done to gain an understanding of the physical processes that occur in the PECSS discharge. The results of the modeling effort and comparison to experimental results are presented.

4.1 Diffusion Model Discussion

There are several plasma, gas collision, and physical constants that will be referenced throughout the diffusion modeling discussion, and they are defined in Table 4-1.

Table 4-1. Diffusion model physical constants.

Physical Constant Description	**Physical Constant Symbol**
Ion Temperature	T_i
Effective Electron Temperature	$T_{e(cold)}$
Primary Electron Number	$\delta(E)$
Spatial Electron/Ion Density	$N_0(x,y,z)$
Neutral Gas Density	N_N
Effective ion or electron collision rate for momentum transfer (frequency)	ν_{mi}, ν_{me}
Effective ion and electron mobilities	μ_i, μ_e
Ionization rate (frequency)	ν_i
Ionization energy (eV per ion electron pair)	ε_i

The equations for the ambipolar diffusion analysis require descriptions of electron collisionality and ion mobility, which are functions of the electron energy distribution. To simplify the analysis, a uniform electron energy distribution at a temperature, T_e, assumed to calculate diffusion coefficients. Prior to introducing the equations of state for the plasma body, four assumptions are made about the conditions of the reactor:

1) neutral gas density and temperature are spatially constant throughout the discharge,
2) the electron and ion temperature are constant in the bulk of the discharge and $T_e >> T_i$,
3) ions are only singly charged and positively charged (i.e. no negative ions), and
4) The sheath can be treated as collisionless or collisional.

With these assumptions one can write out the expressions for ambipolar diffusion of a bounded gas discharge. In this case argon is used for the electropositive plasma since the collision rates and ionization process have been well established for this atomic, noble gas.

4.2. Ambipolar Diffusion Analysis the PECSS Geometry

If an electropositive gas discharge is assumed (i.e. no negative ions such as O^-) where the electron (-) and ion (+) charged-particle concentrations are nearly equal at all points in the interior of the discharge, then it is possible to derive a reasonably good estimation of the spatial profile of charged-particle density and the electron temperature required to sustain ionization rates so as to maintain the discharge in the vessel at a particular pressure. In this first order analysis it is assumed that only single-step ionization from electron-neutral collisions occurs and that electron temperature is spatially uniform. [For some gases this assumption is dubious since many atomic and molecular gases can have significant multi-step ionization pathways through multiple collisions and generation of excited states such as metastable Ar* and He*].

For the purpose of this thesis it is assumed that ionization pathways are of secondary importance and would only result in increased ionization rates when compared to the first order approximation made here. The assumption of uniform T_e is reasonable for collisional plasmas and when the imposed heating electric fields and electron currents are relatively weak. After obtaining a sense of plasma density, collisionality, and electrical conductivity within the first order model, the assumption of uniform electron temperature is re-visited later in this chapter when imposing the external DC fields on the plasma edges. The following analysis concentrates on the bulk body of the plasma in the PECSS volume.

The analysis begins with the classical momentum transfer equations for ions and electrons.

$$\nabla(kT_e N_{e0}) - N_{e0}\vec{F}_{eo} = (N_{e0}V_{eo})m_e\nu_{me} \tag{1}$$

$$\nabla(kT_i N_{i0}) - N_{i0}\vec{F}_{io} = (N_{i0}V_{io})m_i\nu_{mi} \tag{2}$$

In Eq. 1 and 2, k is Boltzman's constant, $\vec{F}$ is the forcing term due to electric fields in the interior of the plasma body, V_{eo}, V_{io} is the net charge particle velocity of electrons and ions, and ν_{me} and ν_{mi} are collision rates of the electrons and ions upon the background neutral gas. Equations 1 and 2 express the momentum transfer of electrons and ions (N_e and N_i) at any point as the balance of thermal diffusion, the influence of any forcing field $\boldsymbol{F}$ (i.e. electric field), and the flux of ion or electrons times the net collision frequency that the electrons or ions experience (drag forces).

Next typical assumptions about the ion temperature and electron temperature are made (or composite electron temperature population) on the scale of a finite element volume.

These approximations allow us to simplify terms for engineering modeling purposes and are listed below.

- Assume that $T_i << T_e$ which is valid for non-thermal, low pressure plasmas.
- Within the local scale of a small but finite volume, the spatial variation of both ion and electron temperatures vary weakly and can be considered as an isotropic constant.

The assumption of isotropic nature of the EEDF (as a Maxwellian distribution) is a greater over-simplification than is the concept of weak spatial variation, particularly if strongly directed primary electrons exist from the plasma cathode sheaths. However, if the primary electrons are a small contributor to the total electron population, then we can proceed with the given two assumptions above, even if spatially varying localized concentrations of primary electrons strongly contribute to local ionization within the PECSS body.

The assumption of near quasi-neutrality (or near equal) ion and electron concentrations is made, $N_{eo} \cong N_{io} = N_o$. This condition is imposed to maintain relatively low space-charge fields (< a few V/cm) within the interior of the plasma body as observed experimentally. Also, the flux of ions and electrons out of any point volume within the plasma is conserved. This ambipolar diffusion condition for a bulk plasma body, where electric fields are generally weak, holds that the flux of ions and the flux of electrons out of any differential volume are approximately equal.

$$\Gamma_e \cong \Gamma_i = \Gamma_o \quad \text{or}$$

$$-N_{e0}\vec{V}_{eo} \cong -N_{i0}\vec{V}_{io}$$

The expressions of ion and electron mobility as they are related to charge-carrier mass, *m*, and the net effective collision frequencies, *v,* are shown in Eq. 3 and 4. For simplicity it is assumed that mobility is a constant and is not dependent upon the local electric field.

$$\mu_e = \frac{e}{m_e \nu_{me}} \tag{3}$$

$$\mu_i = \frac{e}{m_i \nu_{mi}}, \tag{4}$$

Combining these assumptions and expressions for mobility, the momentum transfer equations can be re-expressed with the ambipolar space-charge electric field, $\vec{E}$, used for the forcing term.

$$\frac{1}{m_e \nu_{me}} kT_e \nabla N_{e0} - \mu_e N_{e0} \vec{E} = -\vec{\Gamma}_e \tag{5}$$

$$\frac{1}{m_i \nu_{mi}} kT_i \nabla N_{i0} + \mu_i N_{io} \vec{E} = -\vec{\Gamma}_i \tag{6}$$

Since both ions and electrons are mutually influenced by the plasma electric field, we can further combine Eqs. 5 and 6 to obtain the discharge diffusion equation:

$$\frac{\mu_i \mu_e}{e(\mu_i + \mu_e)} kT_i \nabla N_0 + \frac{\mu_i \mu_e}{e(\mu_i + \mu_e)} kT_e \nabla N_0 = -\vec{\Gamma}_o . \tag{7}$$

By defining the ambipolar diffusion constant, D_a, as

$$D_a = \frac{\mu_i \mu_e}{e(\mu_i + \mu_e)} \cdot kT_e , \tag{8}$$

the combined momentum balance equations for ions and electrons can be expressed as a single equation for charged particle flux.

$$D_a \nabla N_0 (1 + T_i / T_e) \approx D_a \nabla N_0 = -\vec{\Gamma}_o . \tag{9}$$

The next analysis step is to include conservation of mass (or particle generation and loss) by maintaining that the divergence of either ion or electron flux from a local point must be equivalent to the local rate of charged-particle generation. This conservation of particle mass is expressed as

$$\nabla \cdot \vec{\Gamma}_0 = N_0 \nu_i \tag{10}$$

where ν_i is the ionization frequency for single-step ionization. It is noted that for some higher neutral pressure conditions, there may be a net recombination rate, $-N_o \nu_r$, but such rates are not strong for low pressure gases and often involve lower probability three-body reactions. Combining Eqs. 9 and 10 and applying the assumptions above for a differential volume for low pressure plasmas, the classical ambipolar diffusion equation is obtained in Eq. 11.

$$D_a \nabla^2 N_0 + N_0 \nu_i = 0 \tag{11}$$

Since $m_i >> m_e$ and $\nu_{mi} << \nu_{me}$, it generally holds that the electron mobility is much greater than the ion mobility: $\mu_e >> \mu_i$. Thus the diffusion constant D_a can be approximated by

$$D_a = \frac{kT_e \mu_i}{e} \tag{12}$$

and the diffusion equation becomes

$$\frac{kT_e \mu_i}{e} \nabla^2 N_0 + N_0 \nu_i = 0 \tag{13}$$

By applying appropriate boundary conditions, Eq. 13 can be used to spatially calculate ion and electron density within any particular geometry such as a linear hollow cylinder, coaxial cylinder, discharge box, or uniquely shaped body.

The boundary conditions for the system are obtained by setting the current flux at the sheath-plasma edge to the diffusive charged particle flux. At the cathode surfaces, this is given by

$$0.6 \cdot u_B N_0 \cdot \left(1+\gamma_{\sec}\right)\Big|_{C-sheath} = \vec{\Gamma}_o = \hat{n} \cdot -(\gamma_D \cdot D_a)\nabla\left(N_0(x,y,z)\right)\Big|_{C-sheath} \quad (14)$$

where u_B is the "acoustic" speed or Bohm velocity of ions at the edge of the plasma. The value γ_{sec} is the secondary electron yield (typically between 0.05 and 0.01) and γ_D is a correction factor for the ambipolar diffusion constant, D_a, that is applied at the boundary. This adjustment is necessary to account for an increase in ion mobility within the pre-sheath electric field at the sheath edge and to make up for other sheath-plasma edge approximations. In practice the "correction factor", γ_D, is in the range of about 2 to 3 for low pressure argon discharges to match the model predictions to empirical data. For our purposes γ_D was set to three unless mentioned otherwise.

To utilize Eq. 14 with a finite element numerical treatment, an estimator for electron temperature is required. For the present PECSS model, a cold component T_e(Bulk) that is typically on the order of 1 eV exists for the pressures of interest. Primary electrons from secondary emission from cathode walls (300 eV) and scattered electrons, which are born in sheath regions or are the remnant of primary electrons as they are scattered through various inelastic collision processes, are also present.

The approach used to calculate the estimated amplitude of spatial N_0 in a DC plasma case is total DC current conduction. This is given by a more simplified total ion or electron current expressions at the cathode and anode.

$$I_C = \iint_{Cathode} e \cdot 0.6 \cdot u_B N_0(x,y,z) \cdot (1+\gamma_{sec}) dA$$

$$I_A = \iint_{Anode} e \cdot N_0(x,y,z) \cdot \sqrt{\frac{k \cdot T_e}{2 \cdot \pi \cdot m_e}} \cdot \exp\left(\frac{V_A - V_{Plasma}}{T_e}\right) dA$$

The boundary condition enables one to gauge the amplitude of $N_0(x,y,z)$ without having to explicitly account for all loses attributed to multiple pathways of electron sub-gas collisions in the bulk plasma.

For engineering purposes, it is assumed that $V_{Sheath} \approx 0.9 \cdot V_{Cathode}$ given the weak dependency of d_{Sheath} on variation of V_{Sheath}. It is noted that the sheath estimator used here does not include the role of secondary electron emission transport off the cathode surface.

The final step in the analysis sequence is the calculation of collision rates for various ion and electron impact processes. The mobility μ_e and μ_i define the ambipolar diffusion constant, D_a, and the collision frequencies of the ions and electrons define the mobilities and ionization frequencies. While it is possible to calculate these values, there are engineering estimates available in the published literature.

The local ionization rate is defined for the cold bulk electrons and the hot primaries. For cold electrons the ionization rate may be calculated by:

$$\nu_{iCold} = 4.02 \cdot 10^4 \cdot T_e^{1.5} \cdot \exp\left(\frac{-15.7}{T_e}\right) \cdot \left(1 + \frac{7.85}{T_e}\right) \cdot P \cdot \left(\frac{T_{gas}}{295}\right)$$

for cold electron energies between 1 and 10 eV. For hot primary electrons the ionization rate may be approximated by:

$$\nu_{iP} = \sigma_i(eV_{\mathrm{Pr}imaries}) \cdot N_N$$

The production rate of ions is the sum of these ionization rates when multiplied by their respective electron densities N_e(cold) and N_e(primaries) with $eV_{\text{Priamries}} \approx eV_{\text{Cathode}}$.

Electron mobility is mainly derived from elastic collision rates (which dominate electron scattering). However, since $\mu_e >> \mu_i$, electron mobility does not become a significant parameter in diffusive gas-discharge ambipolar diffusion transport.

$$\mu_e = \frac{e}{m_e N_g K_{el}(T_e)}$$

Ion Mobility is the more important term in ambipolar diffusion and is considered constant against gas pressure for relatively low-temperature ions. A reasonable empirical approximation of ion mobility is given by:

$$\mu_i = \frac{e}{M_i N_g K_i} = \frac{e}{M_i N_g \cdot 10^6 \cdot 3.37 \cdot 10^{-16}}$$

Earlier the ambipolar diffusion constant was given as $D_a = kT_e\mu_i/e$ and its value often had to be determined by calculation of ion collision rates. However, other workers have reduced the value of the collision-limited ion mobility to a value that is proportional to both mean-free-ion-path times the Bohm flux:

$$D_a = \left(\frac{T_e}{T_i}\right)^{1/2} \cdot \lambda_i \cdot \mu_B = T_e \cdot \lambda_i \cdot 10^6 \cdot \sqrt{\frac{1}{T_i \cdot M_i}} \qquad \text{(A-3)}$$

where λ_i is the mean-free-path of argon ions in cm and T_i is the ion temperature in eV. The value λ_i for Ar is approximately 1/330 cm at 1 Torr or 1/(330·*P*) cm with *P* in Torr, [Lieberman et al. (1994)].

A unique aspect of the modeling used in this work is an estimate of the spatial distribution of the primary electrons originating as energetic secondaries from the walls of the PECSS cell. We calculate this spatial profile as a weighting function of summed primaries. The weighting function at every point in the volume of the PECSS device is defined as the integrated summation of all vectors from the cathode walls to a point in the discharge volume. In the summation, the contribution of primaries is "attenuated" by a Gaussian function given as:

$$C \cdot \exp\left(\frac{-r^2}{2 \cdot \pi \cdot \sigma^2}\right)$$

where r is the distance between each wall surface point and each internal volume point. The weighting function is designed to simulate the concentration of injection primary electrons from the cathode walls but attenuated by a typical collisional distance. The result of the integration is that primary electrons are more weighted (i.e. concentrated) within the corners and in proximity to the cathode boundaries. The weighting function is normalized to a peak value of 1. An X-Y cross-section of the electron weighting function calculated within the volume of the PECSS geometry is shown in Fig. 4-1 along the center axial z-height of the device. When used in the model, the weighting profile is used to calculate the local concentration of primary electrons:

$$N_{e\,Primary}(x, y, z) = W_e(x, y, z) \cdot N_{e\,Primary} / N_{ecold}$$

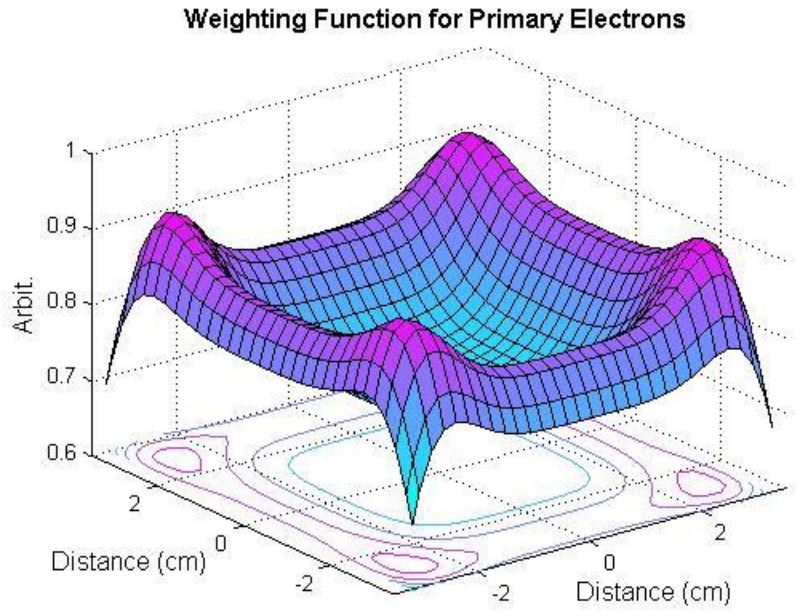

Figure 4-1. Primary electron weighting function (X,Y) used in ambipolar diffusion model as calculated across the Z-mid plane of the PECSS device.

With the ionization frequency terms for cold and primary electrons approximated and the diffusion constant D_a approximated, we may numerically solve the diffusion equation for the PECSS system. The diffusion equation was solved by discretizing the PECSS device geometry in x, y, and z with its center being at (0, 0, 0). The 2^{nd} order differential diffusion equation and the first order differential boundary conditions for ion flux were solved by difference equations using a temporal relaxation method from an initial guess at $N_e(x,y,z)$. In this treatment, we solve only for the relaxation of $N_e(x,y,z)$, but do not re-solve for the weighting function based on a new $N_e(x,y,z)$ value at the PECSS boundaries. Also the value of $N_{ePrimary}/N_e$ is taken as a constant between 0.01 and 0.001 to achieve a satisfactory and realistic range of the total ionization frequency. There is no self-consistent resolution of the primary electron concentration or its spatial distribution, rather the model is intended to see if the bulk diffusion

of ions and cold electrons are impacted by a forced concentration and amplitude of injected primaries.

To illustrate the induced ionization behavior in the model Fig. 4-2 shows the ionization frequency for 200 mT in Ar with $N_{ePrimary}/N_e$ = 0.005 as represented along the mid-plane X-Y cross section of the PECSS device (z=0). Following the weighting function, the ionization frequency peaks at the corners where the injection of high energy primary electrons is apt to be most concentrated. Because primary electron ionization dominates the operation of the PECSS device, the relative shape of the ionization rate profiles in the PECSS device is independent of the pressure.

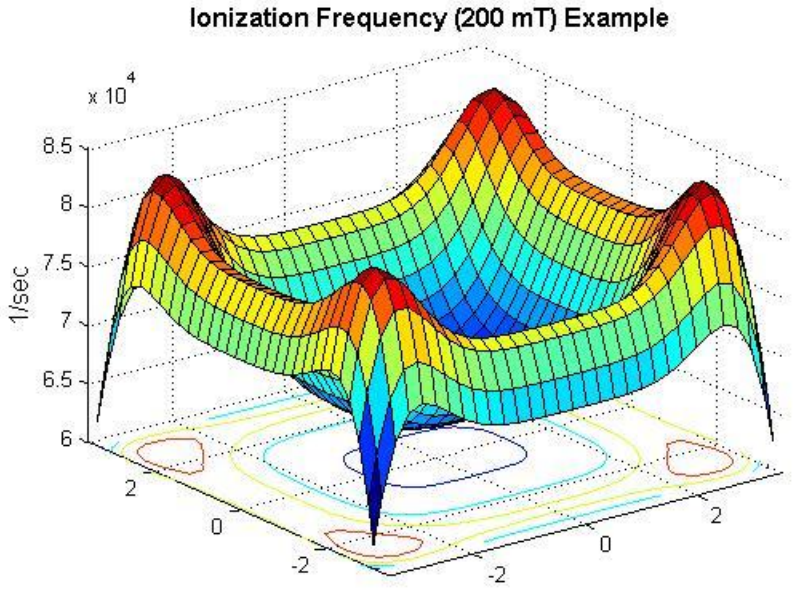

Figure 4-2. Ionization frequency profile in PECSS device. [200 mTorr Argon].

4.3 Numerical Modeling Results

The ambipolar diffusion modeling results support earlier findings described in Chapter 3. The conditions used in the model include ion mobility-limited diffusion and bulk electron temperatures of 1 eV. These two properties were used to calculate the diffusion constant, which was defined in Section 4.2. The model suggests that the ionization in the PECSS device is driven by primary electrons whose energy is on the order of the cathode to anode potential difference and at densities of less than ~0.1% of the bulk electron population. Although the modeling performed in this thesis is not exact, it is able to demonstrate how ionization frequency varies spatially in the pocket controlled by the secondary electron emission from the cathode walls of the PECSS device.

The diffusion modeling results were compared with the strip ion current profiles obtained experimentally and discussed in Section 3.5 of this thesis. The strip ion current and plasma density plots for neutral gas pressures of 100-300 mTorr are shown in Fig. 4-3, 4-4, and 4-5. At a neutral gas density of 100 mTorr the strip ion current does not have peaks as it does at higher pressures. As found experimentally, when low neutral gas pressures are used the strip ion current has only one distinct peak at the middle of the PECSS device. When the neutral gas pressure is increased to 200 or 300 mTorr two distinct peaks appear in the discharge and the ion strip current is lower in the centerline region of the PECSS device where less “nearby” wall surface area is present.

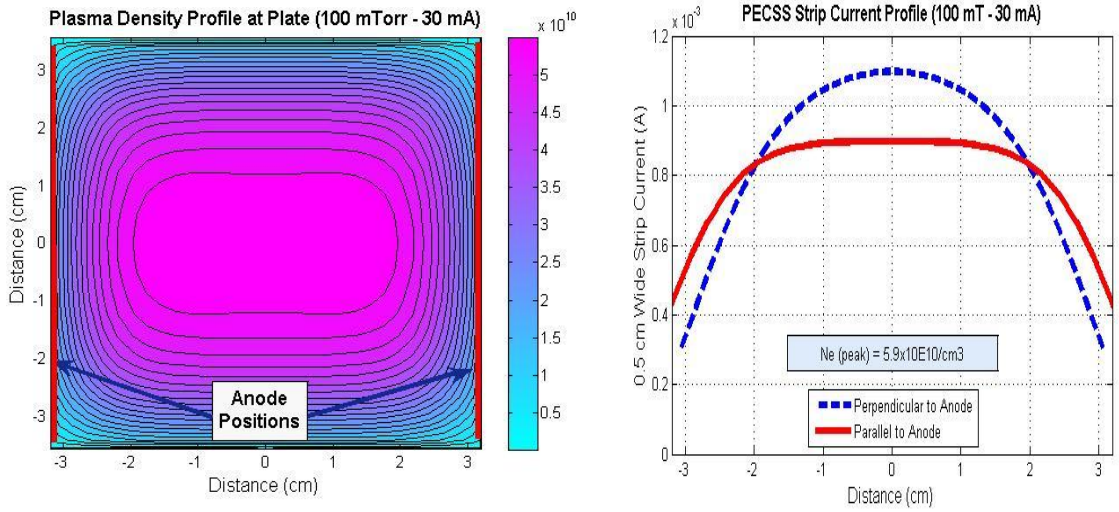

(a) (b)

Figure 4-3. (a) Ionization frequency and (b) strip ion current results from diffusion modeling at 300 V, 30 mA, and 100 mTorr in argon.

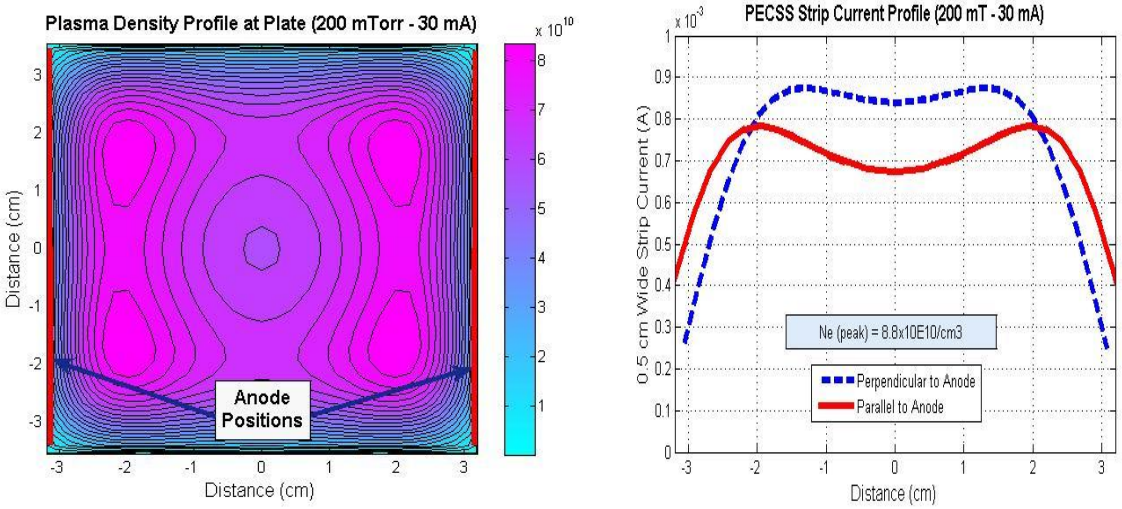

(a) (b)

Figure 4-4. (a) Ionization frequency and (b) strip ion current results from diffusion modeling at 300 V, 30 mA, and 200 mTorr in argon.

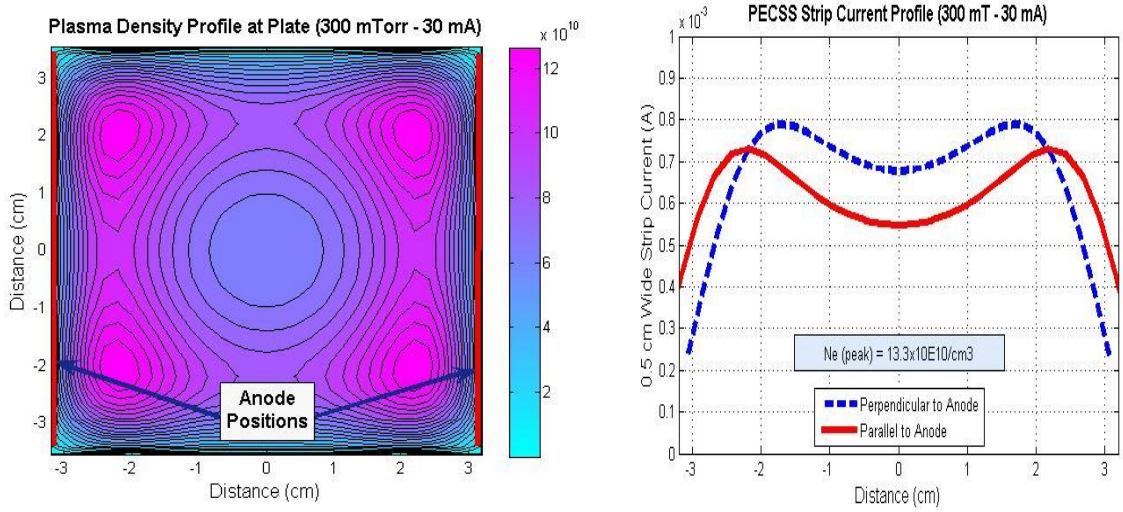

(a) (b)

Figure 4-5. (a) Ionization frequency and (b) strip ion current results from diffusion modeling at 300 V, 30 mA, and 300 mTorr in argon.

The results of the ion current profiles obtained experimentally spatially agree with the ambipolar diffusion results. As in the experiments as the pressure is increased, the peaks in the ion current profiles move toward the walls of the substrates. It is expected that when the molecular gases are used instead of argon the ion current profiles should be more uniform across the substrate. Lighter molecular ions have higher diffusion mobility and also have more complex ionization pathways than the single pathway used with argon in this model [Mahoney, L., private communication (2012)].

CHAPTER 5: CONCLUSION AND FUTURE WORK

This thesis presented plasma properties in the discharge created by a plasma source that was integrated into a close spacing sublimation geometry used in heated pocket deposition processing. The plasma enhanced close spacing sublimation (PECSS) device is applicable to PV manufacturing processes currently in use including plasma cleaning and plasma-enhanced semiconductor deposition.

5.1 Conclusions

Operational characteristics of the PECSS device are presented in this thesis. It is theorized that the low electron group temperature is unable to sustain the discharge, and instead, the primary electrons accelerated from the cathode walls are the main driver of ionization. This premise is supported by a three-dimensional diffusion model in which spatially varying ionization rates are estimated for both primary and bulk plasma electrons.

The electron temperatures in the active discharge region are between 1-5 eV. The density of the plasma in the active discharge region is between 10^{15} and 10^{16} m^{-3}, and increases with increasing discharge current. In the drift plasma region the electron temperatures are a factor of ten lower than in the active plasma region for the same discharge current. Plasma potentials in the active discharge region are a few volts below anode potential, however, in the drift plasma region, the plasma potentials are near the potential of the cathode. This finding suggests that limited plasma production occurs in the drift plasma region, and that it is sustained by ions that are extracted from the active region and drift across the drift plasma region.

When a segmented TCO-coated surface is placed over the PECSS device, ion current could be measured to the segments. The ion current exhibited peaks, occurring approximately at two ionization mean free paths from the side walls before dropping to lower currents in the centerline region. This result is due to the presence of larger numbers of primary electrons in the corners of the PECSS device. In the centerline region there is less nearby wall area, leading to less primary electron concentration, and lower ionization frequency. The peaks in the ion current move toward the wall with increasing neutral gas pressure, as the primary electron mean free path is reduced. It is also noted that regardless of pressure in the PECSS device the percentage of discharge current that strikes the TCO-coated substrate is always about 35%. When a mesh was placed in the PECSS device to create the drift plasma region, the ion current was attenuated by a factor of 5-10. The presence of the mesh results in a more uniform ion current profile over the majority of the substrate. This allows for a more homogeneous treatment of semiconductor films being deposited on the substrate. As the neutral gas pressure in the PECSS device is increased, the ion current is reduced. This result suggests the frequency of ion-neutral scattering and recombination increases in the drift plasma as the neutral density is increased. These collisions will also reduce ion energy and soften the ion assist action on the semiconductor films being deposited. An energetic ion could also charge exchange with a neutral gas atom leading to a low energy ion (that may not flow to the substrate) and a fast moving neutral.

5.2 Future Work

Further characterization of the PECSS device is required to document ion charge state; excited ion, molecule, and atom fluxes; and spatial variation of plasma properties. The PECSS

diagnostic test bed developed during the course of this research allows for characterization of the electron temperature and density throughout the entirety of the source using Langmuir probes placed in many locations. Remote electrostatic analyzer (ESA) and ExB probes could be used to characterize the ion energy and charge states of the plasma. The information collected by the ESA and ExB probes would allow for more detailed descriptions of ion flux and energy striking the walls of the PECSS device. The ion energy distribution and flux are important parameters that affect interactions between the discharge and semiconductor film growth. Improvements to and scaling of the diffusion model to a larger source and verification of the model will allow for greater confidence in the implementation of PECSS within large scale PV module manufacturing lines.

REFERENCES

Anders, A. *Plasma and ion sources in large area coating: A review.* Surface and Coatings Technology, Volume 200, Issues 5-6, pp. 1893-1906 (2005).

Baldwin, M.J., Lynch, T.C., Doerner, R.P., and Yu, J.H. Nanostructure formation on tungsten exposed to low-pressure rf helium plasmas: A study of ion energy threshold and early state growth. Journal of Nuclear Materials, Volume 415, pp. 104-107 (2011).

Barankova, H. and Bardos, L. *Hollow cathode plasma sources for large area surface treatment.* Surface and Coatings Technology, Volume 146-147, pp. 486-490 (2001).

Bardos, L., Barankova, H., and Berg, S. *Thin film processing by radio frequency hollow cathode.* Surface Coatings and Technology, Volume 97, Issues 1-3, pp. 723-728 (1997).

Beal, B.E. *Clustering of Hall Effect Thrusters for High-Power Electric Propulsion Applications.* Ph. D. Dissertation, Department of Aerospace Engineering, University of Michigan (2004).

Bogaerts, A. and Gijbels, R. *Numerical modeling of gas discharge plasmas for various applications.* Vacuum, Volume 69, Issues 1-3, pp. 37-52, (2002).

Chalise, P.R., Watanabe, M., Okino, A., Ko, K., Hotta, E. *Characteristics of an ion induced secondary emission electron gun,* Plasma Sources Science and Technology, Volume 12, pp. 235-244, (2003).

Conrads, H. and Schmidt, M. *Plasma generation and plasma sources.* Plasma Sources Science and Technology. Volume 9, pp. 441-454 (2000).

Croslyn, A.E., Smith, B.W., and Winefordner, J.D. *A Review of Microwave Plasma Sources in Atomic Emission Spectrometry: Literature from 1985 to the Present.* Critical Reviews in Analytical Chemistry, Volume 27, Issue 3, pp. 199-255 (1997).

Farnell, C. Plasma Flow Field Measurments Downstream of a Hollow Cathode. PhD Dissertation, Department of Mechanical Engineering, Colorado State University (2007).

Goebel, D.M., Jameson, K.K., Watkins, R.M., Katz, I., and Mikellides, I.G. *Hollow cathode theory and experiment. I. Plasma characterization using fast miniature scanning probes.* Journal of Applied Physics, Volume 98 (2005).

Gueroult, R., Elias, P.Q., Packan, D., Bonnet, J., and Rax, J.M. *Particle in cell modeling of the observed modes of a dc wire discharge.* Journal of Physics D: Applied Physics, Volume 43, (2010).

Gueroult, R., Elias, P.Q., Packan, D., and Rax, J.M. *A narrow-band, variable energy ion source derived from a wire plasma source.* Plasma Sources Science and Technology, Volume 20, (2011).

Harvey, R.J., Gallagher H.E., and Schumacher, R.E. *Wire-ion-plasma electron gun employing auxiliary grid.* US Patent 4,642,522 (1987).

Hashiguchi, S. Numerical calculations for the electron energy distribution in a helium, hollow-cathode glow discharge. IEEE Transactions on Plasma Science, Volume 19, Issue 2, pp. 297-300 (1991).

Herman, D.A. and Gallimore, A.D. *Discharge Chamber Plasma Structure of a 30-cm NSTAR-type Ion Engine.* AiAA-2004-3794, 40th Joint Propulsion Exhibit, Ft. Lauderdale, FL (2004a).

Herman, D.A. and Gallimore, A.D. Near Discharge Cathode Assembly Plasma Potential Measurements in a 30-cm NSTAR type Ion Engine amidst Beam Extraction. AIAA-2004-3958, Joint Propulsion Conference and Exhibit, Fort Lauderdale, FL (2004b).

Hopwood J. *Review of inductively coupled plasmas for plasma processing.* Plasma Sources Science and Technology, Volume 1, pp. 109-116 (1992).

Johnson, E., Zukotynski, S., and Kherani, N.P. *Operational regimes of the saddle field plasma enhanced chemical vapor deposition system.* J. Vac. Sci. Technol. A, Volume 26, Issue 3, pp. 462-472 (2008).

Joo, J. Numerical modeling of SiH_4 discharge for Si thin film deposition for thin film transistor and solar cells. Thin Solid Films, Volume 519, Issue 20, pp. 6892-6895 (2011).

Koch, H., Friedrich, L.J., Hinkel, V., Ludwig, F., Pollit, B. *Hollow cathode discharge sputtering device for uniform large area thin film deposition.* Journal of Vacuum Science and Technology A, Volume 9, pp. 2374-2377 (1991).

Kutsai, K. and Donko, Z. *Hybrid model of a plane-parallel hollow-cathode discharge.* Journal of Applied Physics, Volume 33, pp. 1081-1089 (2000).

Liberman, M.A. and Lichtenberg, A.J. *Principles of Plasma Discharges and Materials Processing First Edition.* John Wiley & Sons, Inc., Hoboken, New Jersey (1994).

Liberman, M.A. and Lichtenberg, A.J. *Principles of Plasma Discharges and Materials Processing Second Edition.* John Wiley & Sons, Inc., Hoboken, New Jersey (2005).

Lisovskiy, V.A., Yakovin, S.D., and Yegorenkov, V.D. *Low-pressure gas breakdown in uniform dc electric field.* Journal of Physics D: Applied Physics, Issue 33, pp. 2722-2730 (2000).

Mahoney, L. Private Communication (2012).

Makarov, M., Loumani, Y., Minea, T., Gousset, G., and Kozyrev, A. *Why does a low-pressure wire-discharge exist self-sustained?* Europhysics Letters, Volume 74, Number 3, pp. 431-437, (2006).

McClure, G.W. *Low-Pressure Glow Discharge.* Applied Physics Letters, Volume 2, Number 12, pp. 233-234 (1963).

McIlraith, A.H. *A Charged Particle Oscillator.* Nature, Volume 212, pp. 1422-1424 (1966).

Rech, B., Roschek, T., Repmann, T., Muller, J., Schmitz, R., and Appenzeller, W. *Microcrystalline silicon for large are thin film solar cells.* Thin Film Solids, Volume 427, Issues 1-2, pp. 157-165 (2003).

Riedel, N.A. Plasma processing for nanostructured topographies. Ph.D. Dissertation (2012).

Riedel, N.A., Cote, T.B., Bechara, S.L., Popat, K.C., and Williams, J.D. *Low energy helium ion texturization of titanium and relevance to biomedical applications.* Surface and Coatings Technology, Volume 206, Issue 23, pp. 4750-4755 (2012)

Sagnes, E., Szurmak, J., Manage, D., and Zukotynski, S. *Structure of hydrogenated amorphous carbon deposited using saddle-field glow-discharge in methane*. Journal of Non-Crystalline Solids, Volume 249, Issue 1, pp. 69-79 (1999).

Schrittwieser, R., Ionita, C., Murawski, A., Maszl, C., Asandulesa, M., Nastuta, A., Rusu, G., Douat, C., Olenici, S.B., Vojvodic, I., Dobromir, M., Luca, D., Jaksch, S., and Scheier, P. *Cavity-hollow cathode-sputtering source for titanium films*. Journal of Plasma Physics, Volume 76, Issues 3-4, pp. 655-664, (2010).

Shah, A., Torres, P., Tscharner, R., Wyrsch, N., and Keppner, H. *Photovoltaic Technology: The Case for Thin-Film Solar Cells.* Science, Volume 285, pp. 692-698 (1999).

Silva, M.A.M, Martinelli, A.E., Alves Jr., C., Nascimento, R.M., Tavora, M.P., and Vilar, C.D. *Surface modifications of Ti implants by plasma oxidation in hollow cathode discharge.* Surface and Coatings Technology

Singh, B., Mesker, O.R., Levine, A.W., and Arie, Y. *Hollow cathode plasma assisted chemical vapor deposition of diamond.* Applied Physics Letters, Volume 52, pp. 1658-1660 (1988).

Smirnov, A., Raitses, Y., and Fisch, N.J. *Plasma measurements in a 100 W, cylindrical Hall thruster.* Journal of Applied Physics, Volume 95, Number 5, pp. 2283-2292 (2004).

Swanson, D.E., Lutze, R.M., Sampath, W.S., and Williams, J.D. *Plasma Cleaning of TCO Surfaces Prior to CdS/CdTe Deposition.* Proceedings of the 38th Photovoltaic Specialists Conference (2012a).

Swanson D.E., McGoffin, G., Geisthardt, R., Williams, J.D., and Sites. J. *Improved CdTe Solar-cell Performance by Plasma Cleaning the TCO.* To be submitted to Progress in Photovoltaics (2012b).

Swanson, D.E. *Development of plasma cleaning and plasma enhance close space sublimation hardware for improving CdS/CdTe solar cells.* Masters Thesis, Department of Mechanical Engineering, Colorado State University (2012).

Tanarro, I., Herrero, V.J., Carrasco, E., and Jimenez-Redondo, M. *Cold Plasma Chemistry and Diagnostics.* Vacuum, Volume 85, Issue 12, Pages 1120–11245, (2011).

Urai, H., Kurosawa, T., Akitoshi, O., Hotta, E., Yasui, H., Tamagawa, T., and Ko, K. *High-repetition-rate operation of the wire ion plasma source using a novel method.* Rev. Sci. Instrum. Volume 68, Issue 9, pp. 3346-51, (1997).

Williams, J.D. *An Experimental Investigation of Hollow Cathode-Based Plasma Contactors.* PhD Dissertation, Department of Mechanical Engineering, Colorado State University (1991).